

OPTIMAL AQUIFER MANAGEMENT FOR  
CONTROLLING LAND SUBSIDENCE

*Lu-chia Chuang*  
**Optimal Aquifer Management for Controlling Land Subsidence**

*[Signature]*  
Chairman of the Committee  
Frederick G. Cleveland,  
Assistant Professor,  
Civil and Environmental Engineering  
**A Thesis Presented to  
the Faculty of the Interdisciplinary Graduate  
Program in Environmental Engineering  
University of Houston**

*[Signature]*  
Jerry R. Rogers,  
Associate Professor,  
Civil and Environmental Engineering  
**In Partial Fulfillment  
of the Requirements for the Degree  
Master of Science in Environmental Engineering**

*[Signature]*  
**by  
Lu-chia Chuang  
May 1993**

*[Signature]*  
Assistant Professor,  
Industrial Engineering

*[Signature]*  
James M. Symons,  
Professor and Director,  
Civil and Environmental Engineering

OPTIMAL AQUIFER MANAGEMENT FOR  
CONTROLLING LAND SUBSIDENCE

Lu-chia Chuang

Lu-chia Chuang

Approved:

Theodore G. Cleveland

Chairman of the Committee  
Theodore G. Cleveland,  
Assistant Professor,  
Civil and Environmental Engineering

Committee Members :

Jerry R. Rogers

Jerry R. Rogers,  
Associate Professor,  
Civil and Environmental Engineering

Lawrence J. H. Schulze

Lawrence J. H. Schulze,  
Assistant Professor,  
Industrial Engineering

Charles Dalton

Charles Dalton  
Associate Dean  
Cullen College of Engineering

James M. Symons

James M. Symons  
Professor and Director  
Civil and Environmental Engineering

## ACKNOWLEDGEMENTS

I gratefully acknowledge my research advisor, Dr. Theodore G. Cleveland, for his advice, support and guidance throughout the course of this project.

I would also like to thank Dr. Jerry R. Rogers, and Dr. Lawrence J. H. Schulze for reviewing this document.

I would like to express my appreciation to Mr. Bud Holschuz of the Harris-Galveston Coastal Subsidence District for his help during this project.

Finally, I would like to thank my family for their love that support throughout my education.

Presented to

the Faculty of the Interdisciplinary Program in Environmental Engineering

University of Houston

In Partial Fulfillment

of the Requirements for the Degree

Master of Science in Environmental Engineering

by

Li-chia Chang

May 1993

ABSTRACT

**OPTIMAL AQUIFER MANAGEMENT FOR CONTROLLING  
LAND SUBSIDENCE**

The study involved the creation of a three-dimensional groundwater model, calibration and verification of the model, coupling of the model to a generalized nonlinear optimization code, and testing of the combined model for existing conditions.

An Abstract of a Thesis

Presented to

the Faculty of the Interdisciplinary Program in Environmental Engineering

University of Houston

The objectives of this study are the following: (1) It determines the total subsidence in the region; and (2) it reduces energy usage without affecting ground water delivery.

A data regeneration method to regenerate the missing data in the model was developed in this study. The method is based on the probability distribution of original data to regenerate missing elements. The regenerated data is compared to the original data.

In Partial Fulfillment

of the Requirements for the Degree

Master of Science in Environmental Engineering

The results show that relatively subtle changes in pumping distribution can significantly affect subsidence patterns and dramatically reduce pumping costs.

by

Lu-chia Chuang

May 1993

## ABSTRACT

Page

The objectives of this study were to apply simulation and optimization techniques to explore management strategies that minimize land subsidence and energy consumption while satisfying ground water demand. The study involved the creation of a three-dimensional flow and subsidence model, calibration and verification of the model, coupling of the model to a generalized nonlinear optimization code, and testing of the combined simulation-optimization model for existing conditions. ....

The model has been used in the Houston-Galveston region to minimize the effect of ground water discharge. The model also can be used to minimize energy usage without reducing the ground water discharge. The pumping policy of this model compared with the historical pumping policy in the Houston-Galveston area are the following: (1) It successfully reduces the total subsidence in the region; and (2) it reduces energy usage without compromising ground water delivery. ....

Also an effective, but simple, data regeneration method to regenerate the missing sand fractions in the aquifer model was developed in this study. The method is based on the probability mass function of sand fractions of the original data to regenerate missing elements. The regenerated model has a closer statistical agreement to the original data than regeneration by other geostatistical methods. ....

The results indicate that relatively subtle changes in pumping distributions can significantly affect subsidence patterns and dramatically reduce pumping costs. ....

Horizontal Geological Parameters ..... 20

Ground Water Pumpage ..... 24

## TABLE OF CONTENTS

	Page
ACKNOWLEDGMENTS.....	i
ABSTRACT.....	ii
LIST OF FIGURES.....	vi
LIST OF TABLES.....	viii
<b>Chapter 1 Introduction.....</b>	<b>1</b>
<b>Chapter 2 Literature Review.....</b>	<b>6</b>
Ground Water/Subsidence Model in the Houston-Galveston Region.....	6
Ground-Water Management/Optimization.....	7
<b>Chapter 3 Ground-Water Flow and Land Subsidence Model.....</b>	<b>9</b>
Introduction.....	9
Conceptual Aquifer Model.....	10
Conceptual Subsidence Model (Interbed).....	10
Incorporating Storage Changes into the Ground Water Flow Model.....	13
Parameters in the Model.....	14
Procedures.....	15
<b>Chapter 4 Houston-Galveston Ground Water Aquifer Model.....</b>	<b>20</b>
Introduction.....	20
Model.....	20
Horizontal Geological Parameters.....	20
Ground Water Pumpage.....	24
<b>Chapter 5 Summary and Conclusions.....</b>	<b>74</b>
<b>References.....</b>	<b>76</b>

<b>Chapter 5</b>	<b>Interbed Storage Coefficients</b> .....	25
	Introduction.....	25
	Sand Fraction Type.....	25
	Element Type.....	26
	Regeneration Methods.....	27
	Stochastic Regeneration Method.....	35
	Interbed Storage Coefficient.....	37
<b>Chapter 6</b>	<b>Calibration</b> .....	43
	Introduction.....	43
	Simulation Period.....	43
	An Incorrect Model.....	43
	The Second Calibration.....	46
<b>Chapter 7</b>	<b>Optimization</b> .....	53
	Introduction.....	53
	Mathematical Model.....	53
	GRG2.....	54
	Aquifer Optimization Simulator.....	56
	Test Problem.....	56
<b>Chapter 8</b>	<b>Optimal Subsidence Simulation</b> .....	61
	Ground Water Simulation.....	61
	Minimum Subsidence Simulation.....	61
	Minimum Energy Simulation.....	63
	Comparisons.....	63
<b>Chapter 9</b>	<b>Summary and Conclusions</b> .....	74
<b>References</b>	.....	76
	Comparison of Subsidence between Real Data and Simulation Data in Row 5.....	48

## LIST OF FIGURES

FIGURE	Page
1-1 Regional Map and Line of Geologic Section.....	2
1-2 Hydrologic Profile from Montgomery County to Texas City.....	3
3-1 Aquifer Unit Schematic Diagram .....	9
3-2 Conceptual Model of the Ground Water Hydrology of the Houston-Galveston Area.....	11
3-3 Location of Modeling Area.....	17
3-4 Flowchart.....	19
4-1 Locations of Bravo's Modeling Area .....	21
4-2 Estimated Transmissivity and Storage Coefficient of the Chicot Aquifer.....	22
4-3 Estimated Transmissivity and Storage Coefficient of the Evangeline Aquifer .....	23
5-1 Original Sand Fraction Distribution Map of the First Layer.....	28
5-2 Stochastic Regenerated Sand Fraction Map of the First Layer.....	29
5-3 Kriging Regenerated Sand Fraction Map of the First Layer.....	30
5-4 Linear Interpolation Regenerated Sand Fraction Map of the First Layer.....	31
5-5 Flowchart of the Stochastic Regeneration Method .....	36
5-6 Soil Profile - Clear Lake.....	38
5-7 Soil Profile - Southwest Area.....	39
5-8 Soil Profile - Baytown Area.....	40
5-9 Relationship between Vertical Hydraulic Coefficients and Sand Fraction.....	42
6-1 Ground Water Withdrawals in the Houston-Galveston Region, 1978-1987.....	44
6-2 Approximate Land-surface Subsidence, 1978-1987 .....	45
6-3 Simulation of Subsidence from 1978-1987 .....	47
6-4 Comparison of Subsidence between Real Data and Simulation Data in Row 5.....	48



6-5	Comparison of Subsidence between Real Data and Simulation Data in Row 6.....	48
6-6	Comparison of Subsidence between Real Data and Simulation Data in Row 7.....	49
6-7	Comparison of Subsidence between Real Data and Simulation Data in Row 8.....	49
6-8	Comparison of Subsidence between Real Data and Simulation Data in Row 9.....	50
6-9	Comparison of Subsidence between Real Data and Simulation Data in Row 10 ...	50
6-10	Comparison of Subsidence between Real Data and Simulation Data in Row 11 ...	51
6-11	Comparison of Subsidence between Real Data and Simulation Data in Row 12 ...	51
7-1	Flowchart of GRG2 (modified from Lansey & Mays 1989).....	55
7-2	Flowchart of the Optimal Simulator.....	57
7-3	The One-layer Homogenous Aquifer Test Problem.....	58
7-4	Pump Distribution of the Aquifer before Optimization.....	59
7-5	Pump Distribution of the Aquifer after Optimization.....	60
8-1	Initial Subsidence Distribution.....	62
8-2	Simulated Subsidence Distribution (Minimum Subsidence) .....	64
8-3	Surface Plot of Initial Subsidence .....	65
8-4	Surface Plot of Minimum Subsidence Simulation.....	66
8-5	Surface Plot of The Difference between Initial Subsidence and Minimum Subsidence Simulation.....	67
8-6	Change of Pumping Rate between Initial Subsidence and Minimum Subsidence Simulation.....	68
8-7	Simulated Subsidence Distribution (Minimum Energy) .....	69
8-8	Comparison of Subsidence in Row 8.....	71
8-9	Comparison of Subsidence in Row 9.....	71
8-10	Comparison of Subsidence in Row 10 .....	72
8-11	Comparison of Subsidence in Row 11 .....	72
8-12	Comparison of Subsidence in Row 12 .....	73

## LIST OF TABLES

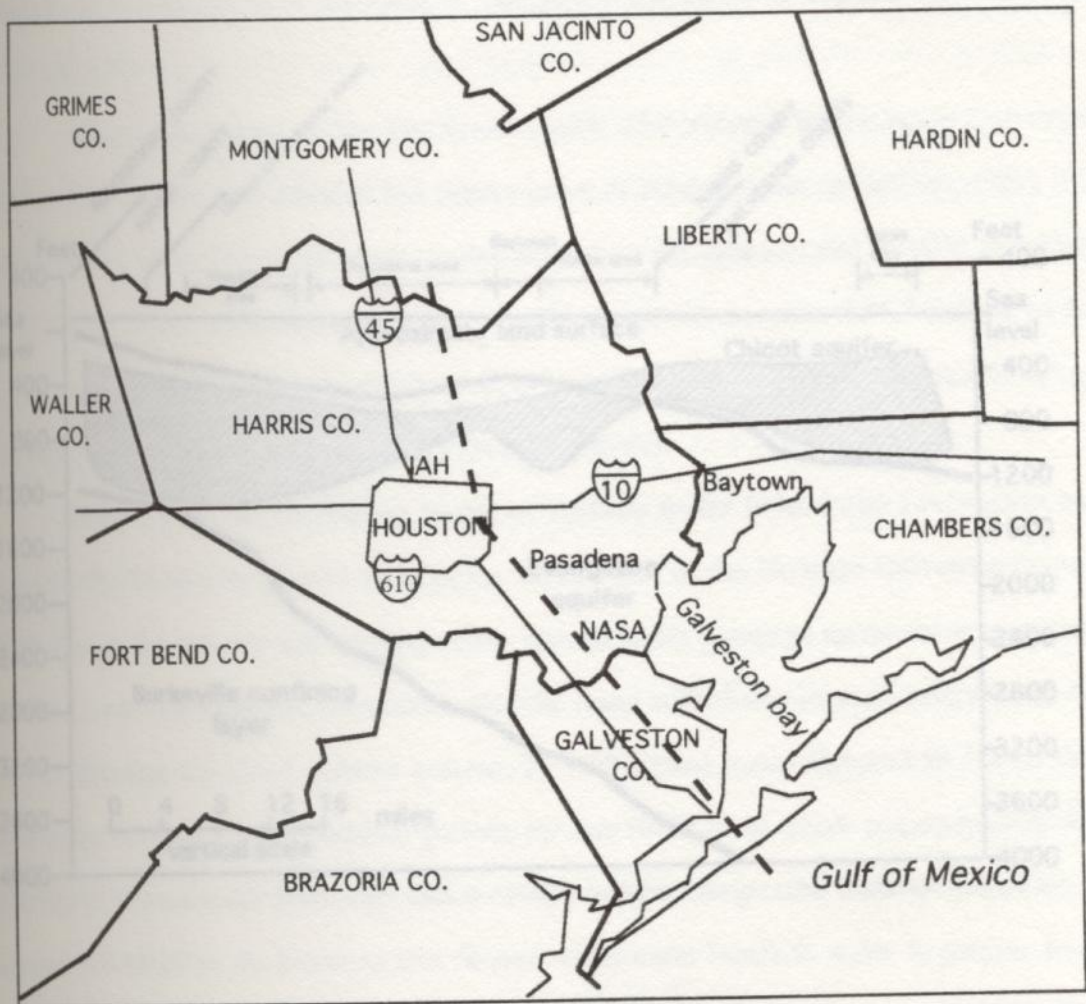
TABLE	Page
3-1 Sources and Methods to Obtain Parameters.....	15
5-1 Range of the Sand Fraction .....	26
5-2 Three Types of Elements .....	26
5-3 Comparison of Sand Fraction Appearance Percentage.....	27
5-4 Conditional Distribution of the Original Sand Fraction Map.....	32
5-5 Conditional Distribution of the Sand Fraction Map Using Stochastic Method.....	32
5-6 Conditional Distribution of the Sand Fraction Map Using Kriging Method.....	33
5-7 Conditional Distribution of the Sand Fraction Map Using Linear Interpolation ....	33
5-8 Results of the Z-test.....	34
5-9 P-Value.....	34
5-10 Interbed Storage Coefficients Obtained from Extensometer Sites .....	41
8-1 Comparison of Subsidence between Three Models .....	70

pumping of ground water in this region has resulted in ground water elevation declines of  
 20 ft (6 m) in wells of the Chicot aquifer and 300 ft (91 m) in wells of the Brazos  
 aquifer (Bravo, 1990). The ground water withdrawals cause the compressible layers to  
 consolidate resulting in subsidence. More than 4500 square miles of land have had one foot  
 or more of subsidence (Gabrysch and Bouquet, 1975). The area of major subsidence has  
 been the Pasadena area (near the Houston Ship Channel) with more than 10 ft (3 m) of  
 subsidence from 1943 to 1978 (Gabrysch, 1984). The Baytown-LaPorte area has subsided  
 9.1 ft (2.8 m) during 1915-1978. The Texas City area has as much as 6 ft (1.8 m) of  
 subsidence. Other less obvious subsidence areas include downtown Houston with more  
 than 4 ft subsidence, Bellonte with 3.5 ft, the Galena area with one foot since 1973, and  
 Lake Houston Dam which has subsided more than 2 feet since 1954.

## Chapter 1 Introduction

The Houston-Galveston region is located in southeastern Texas near Galveston and Trinity Bays and the Gulf of Mexico. The area includes all of Houston, most of Galveston County, and parts of Fort Bend, Chambers, Liberty, and Waller Counties (Figure 1-1). The elevation of downtown Houston is about 49 ft (15 m) above mean sea level. The southern region is vulnerable to tidal flooding. Land subsidence compounds flood damage, as well as causes other damage.

The major ground water supply aquifer units in the Houston-Galveston region are the Chicot and the Evangeline aquifers (Jorgensen, 1975), as shown on Figure 1-2. The Chicot aquifer overlies the Evangeline aquifer, which is underlain by the Burkeville confining layer. Both aquifers consist of unconsolidated and discontinuous layers of sand and clay that dip toward the Gulf of Mexico. During the past 80 years, the region has pumped more ground water from the aquifers than is recharged by annual rainfall (Harris-Galveston Coastal Subsidence District, 1981). In the last five decades alone, the heavy pumping of ground water in this region has resulted in ground water elevation declines of 250 ft (76 m) in wells of the Chicot aquifer and 300 ft (91 m) in wells of the Evangeline aquifer (Bravo, 1990). The ground water withdrawals cause the compressible layers to consolidate resulting in subsidence. More than 4500 square miles of land have had one foot or more of subsidence (Gabrysch and Bonnet, 1975). The area of major subsidence has been the Pasadena area (near the Houston Ship Channel) with more than 10 ft (3 m) of subsidence from 1943 to 1978 (Gabrysch, 1984). The Baytown-LaPorte area has subsided 9.1 ft (2.8 m) during 1915-1978. The Texas City area has as much as 6 ft (1.8 m) of subsidence. Other less obvious subsidence areas include downtown Houston with more than 4 ft subsidence, Bellaire with 3.5 ft, the Galleria area with one foot since 1973, and Lake Houston Dam which has subsided more than 2 feet since 1954.



--- hydrologic profile line

Figure 1-1 Regional Map and Line of Geologic Section

The principal problems caused by land subsidence are: (1) Differential changes in elevation and profiles of stream channels, ditches, and water transport structures; (2) failure of water-well casings due to compressive stresses generated by compaction of aquifer system; (3) tidal encroachment in lowland coastal areas; and (4) in areas of intensive subsidence, development of tensile or compressional stress in engineering structures (Pined, 1964).

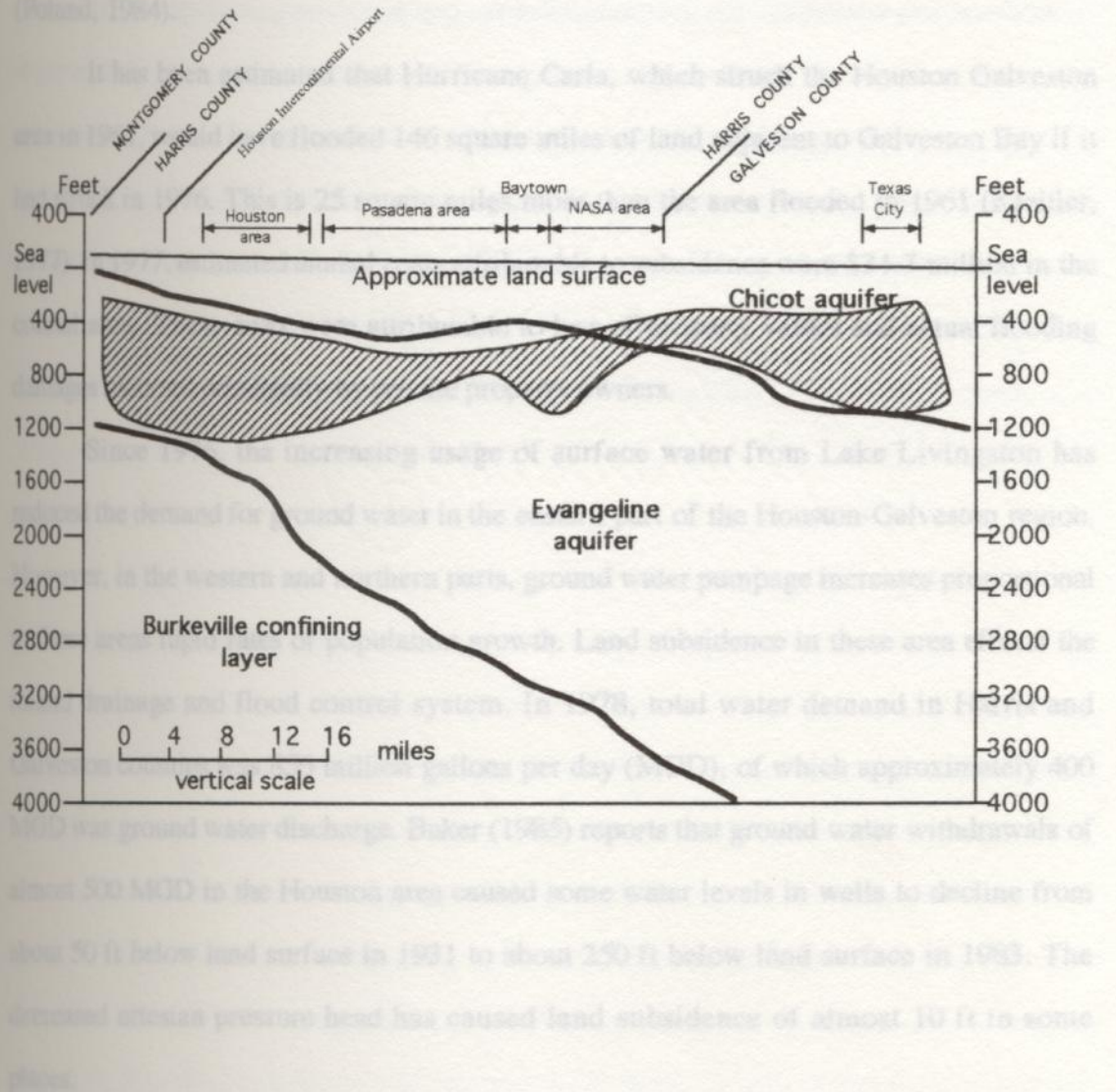


Figure 1-2 Hydrologic Profile from Montgomery County to Texas City (modified from Gabrysch, 1975)

The principal problems caused by land subsidence are: (1) Differential changes in elevation and gradient of stream channels, drains, and water-transport structures; (2) failure of water-well casings due to compressive stresses generated by compaction of aquifer systems; (3) tidal encroachment in lowland coastal areas; and (4) in areas of intensive subsidence, development of tensional or compressional strain in engineering structures (Poland, 1984).

It has been estimated that Hurricane Carla, which struck the Houston Galveston area in 1961, would have flooded 146 square miles of land adjacent to Galveston Bay if it had struck in 1976. This is 25 square miles more than the area flooded in 1961 (Kreitler, 1977). In 1977, estimated annual costs attributable to subsidence were \$31.7 million in the coastal area. These costs were attributable to loss of property values and actual flooding damages incurred principally by private property owners.

Since 1976, the increasing usage of surface water from Lake Livingston has reduced the demand for ground water in the eastern part of the Houston-Galveston region. However, in the western and northern parts, ground water pumpage increases proportional to these areas rapid rates of population growth. Land subsidence in these area effects the inland drainage and flood control system. In 1978, total water demand in Harris and Galveston counties was 856 million gallons per day (MGD), of which approximately 400 MGD was ground water discharge. Baker (1985) reports that ground water withdrawals of almost 500 MGD in the Houston area caused some water levels in wells to decline from about 50 ft below land surface in 1931 to about 250 ft below land surface in 1983. The decreased artesian pressure head has caused land subsidence of almost 10 ft in some places.

The Houston-Galveston region cannot successfully continue its growth unless there is development of ground water management in the Texas coastal area and surface water supplies are accelerated. To develop ground water supplies, the impact of land subsidence

due to the compaction of clayey layers in the two major ground water supply aquifers, should be considered.

The objectives of this study are to apply simulation and optimization techniques to explore management strategies that minimize land subsidence and energy consumption while satisfying ground water demand. The study involved several features: (1) The creation of a three-dimensional flow and subsidence model; (2) calibration and verification of the model; (3) coupling of the model to a generalized nonlinear optimization code; and (4) testing of the combined simulation-optimization model for existing conditions.

The results indicate that relatively subtle changes in pumping distributions can significantly affect subsidence patterns and dramatically reduce pumping costs.

## Chapter 2 Literature Review

This section briefly reviews modeling efforts of the Houston-Galveston region and also the general subject of ground water management.

### Ground Water/Subsidence Model in Houston-Galveston Region

Jorgensen (1975) used an electrical analog model to simulate the hydrologic conditions of the aquifers in the Houston area. The models covered an area of 9,100 square miles with the grid space of 1 square mile. Jorgensen's study provided a means for forecasting declines of ground water head under various conditions of pumping. Jorgensen concluded that both land subsidence and salt-water encroachment could be reduced by artificially recharging the artesian part of the aquifer. However, his study was not designed to predict subsidence.

A digital model to simulate hydrologic conditions in the Chicot and Evangeline aquifers in Houston area was developed by Meyer and Carr in 1979. The ground water system in their study was modeled as a 63-column by 67-row by 5-layer model. The model consists of an area of 27,000 square miles. Finite difference methods were used to solve the system.

In 1988, Ryder studied hydrogeology and predevelopment flow in the Texas Gulf Coast aquifer system. His study model covered of an area of 230,000 square miles on-shore and about 65,000 square miles off-shore. The purposes of Ryder's study were to define the hydrogeologic framework and hydraulic characteristics of the aquifer systems, delineate the extent of freshwater and density of saline water in the various hydrogeologic units, and describe the regional ground water flow system.



Bravo in 1990 used a digital computer model to simulate hydrologic conditions and to predict land subsidence in the Houston-Galveston region. In his study, a grid pattern of 15-column by 15-row by 4-layer was used to represent an area of 5,625 square miles. The discharge rates in the simulation varied from 392 millions gallons per day to 493 MGD. Bravo's conceptual ground water model was solved using the Modular Three-Dimensional Finite-Difference Ground-Water Flow Model (MODFLOW, 1988) and Interbed-Storage Package (Leake & Prudic, 1991). Bravo's model performed well in predicting piezometric head in the Chicot and Evangeline aquifers. Also, land subsidence can be estimated in his model. However, the obvious extensions of this model to aquifer management was never explored.

#### Ground-Water Management/Optimization

An optimal control model for ground water management was developed by Casola, Duffy, and Bishop (1986). Their management model integrated a physically-based finite-difference aquifer simulation model and a linear-quadratic optimal control model.

Wanakule, Mays, and Lasdon (1986) developed an optimal management method to simulate large-scale ground-water aquifers. A finite-difference method was used to simulate ground-water flow. Ground-water optimization was solved by nonlinear programming using the generalized reduced gradient method (GRG2). However, the study did not apply to land-surface subsidence.

In 1990, Duan, Mays, and Lansey developed a reliability-based optimization model for water-distribution systems. The model was developed to determine the optimal operation of the water pumping and tank system. The nonlinear programming problem was solved using GRG2. Again, this study did not apply to land-surface subsidence.

A study of regionally optimal ground-water extraction strategies has been developed by Peralta and Datta (1991). The goals of the study were to maximize total pumpage and to maintain a prespecified target potentiometric surface. The study area was modeled into a one-layer aquifer system.

The ground-water system in the Houston-Galveston region is conceptualized as a multi-layered aquifer system with interbedded compressible layers. The schematic shown in Figure 3-1 is an aquifer unit with interbedded compressible layers. The homogeneous aquifer material and the compressible interbedded layers are two assumptions of the aquifer system.

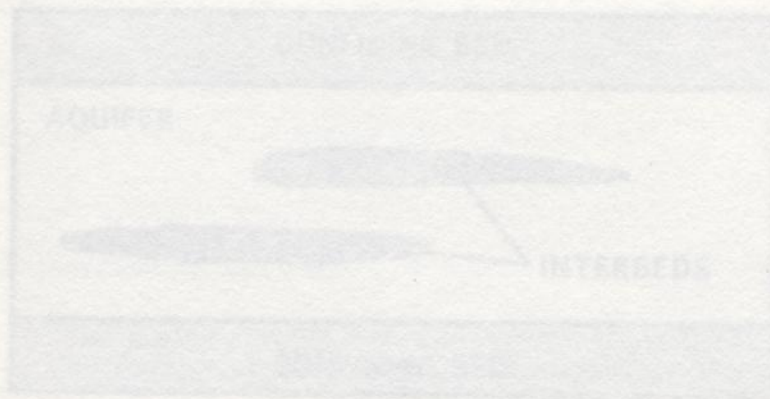


Figure 3-1. Aquifer Unit Schematic Diagram

The numerical implementation of the simulation model is accomplished using the Interbed Storage Module (Leaky and Prodic, 1991) that is attached to the United States Geological Survey (U.S.G.S.) Modular Three-dimensional Finite-Difference Ground-Water Flow Model (McDonald and Harbaugh, 1988).

## Chapter 3 Ground-Water Flow and the Land Subsidence Model

### Introduction

The ground water system in the Houston-Galveston region is conceptualized as a multi-layered aquifer system with interbedded compressible layers. The illustration shown as Figure 3-1 is an aquifer unit with interbedded compressible layers. The incompressible aquifer material and the compressible interbedded layers are two assumptions of the aquifer system.

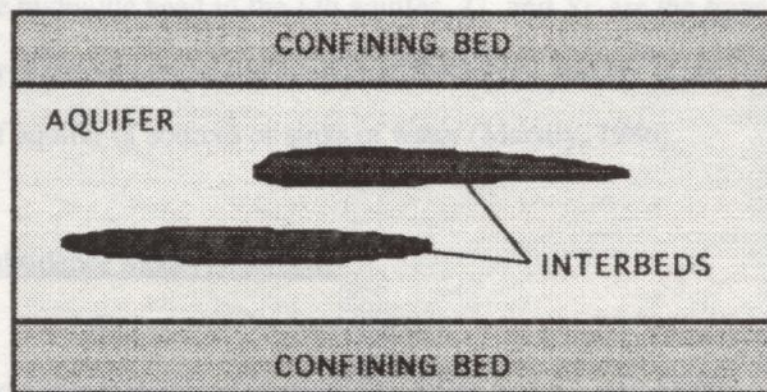


**Figure 3-1.** Aquifer Unit Schematic Diagram

The numerical implementation of the simulation model is accomplished using the Interbed Storage Module (Leaky and Prudic, 1991) that is attached to the United State Geological Survey (U.S.G.S.) Modular Three-dimensional Finite-Difference Ground-Water Flow Model (McDonald and Harbaugh, 1988).

### Conceptual Aquifer Model

The Chicot aquifer was modeled as anisotropic aquifer with the potential for either confined or unconfined horizontal flow. The Evangeline aquifers were modeled as confined leaky anisotropic aquifers (Figure 3-2).

The governing equation of horizontal ground water flow in any of the isotropic aquifer layers is

$$\text{div} ( T_i \text{grad} ( h_i ) ) - W_i = S_i \frac{\partial h_i}{\partial t}, \quad (3-1)$$

where  $h_i$  is the hydraulic head in the  $i$ -th aquifer,  $T_i$  and  $S_i$  are the transmissivity tensor and the aquifer storativity in the  $i$ -th aquifer, respectively, and  $W_i$  is the volumetric flux per unit volume of aquifer of sources or sinks of water (Marsily, 1986).

### Conceptual Subsidence Model (Interbed)

Ground water is removed from storage when water is pumped from aquifers. Jacob (1940) postulated that stored water in confined aquifers is derived from the expansion of water and the compression of the clayey beds that are adjacent to and within the aquifer. He later concluded that the principal source of stored water is from the compression of the clayey beds.

Compression or compaction of the sediments is elastic if the lowering of fluid (pore) pressures does not result in permanent rearrangement of the structure of the sediments and if water removed from storage can be replaced when fluid pressures increase. However, if the fluid pressures decrease beyond the interval where the sediments compact elastically, additional water is released from the clayey beds as skeletal structure is

arranged and permanently compacted. This process is referred to as permanent or elastic compression.

The term "inerted" is used in this thesis to denote a poorly permeable bed within a relatively permeable aquifer. Such beds are assumed to be as follows: (1) of significantly lower hydraulic conductivity than the surrounding aquifer; (2) of head change that is significantly smaller than that of the surrounding aquifer; (3) of a thickness that is relatively small compared to the horizontal extent. The interbedded beds have relatively low permeability so that

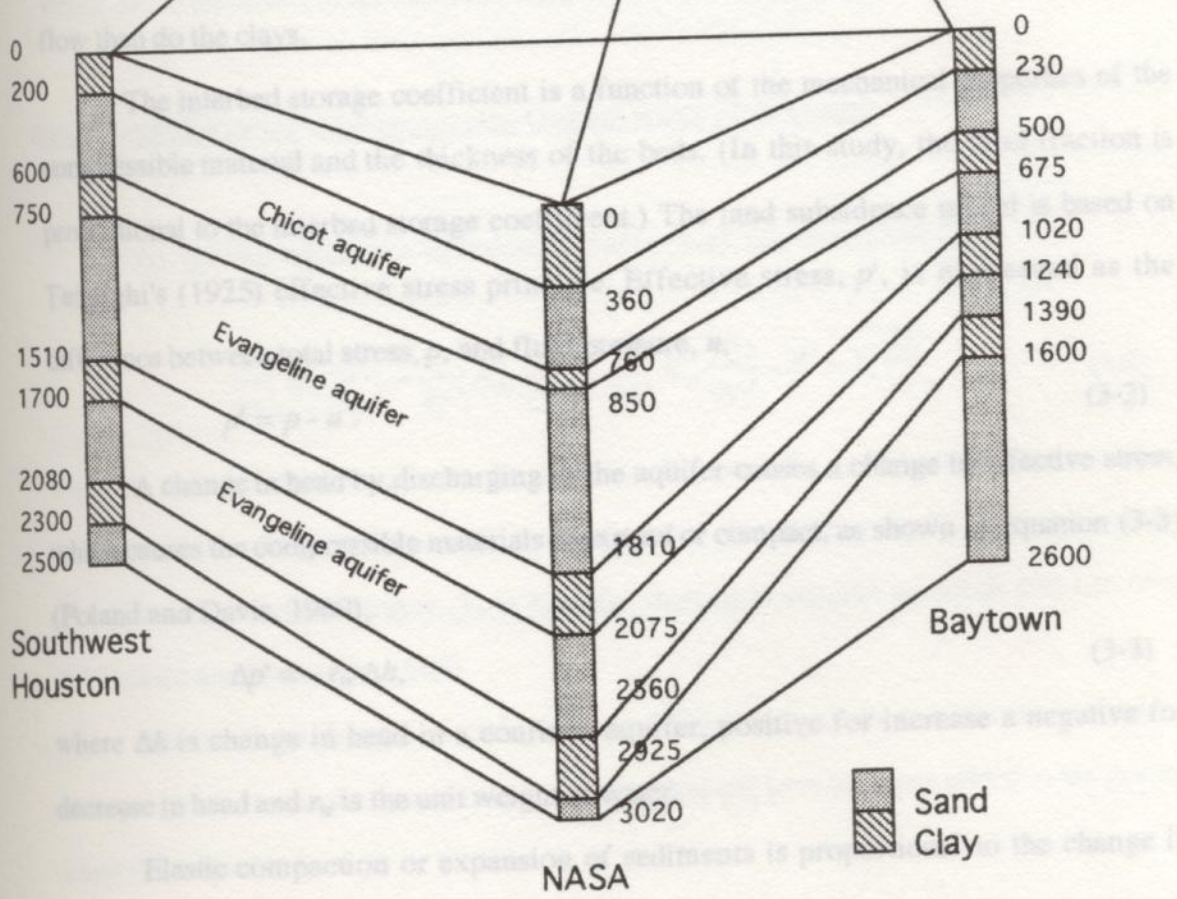


Figure 3-2 Conceptual Model of the Ground Water Hydrology of the Houston-Galveston Area

rearranged and permanently compacted. This process is referred to as permanent or inelastic compaction.

The term "interbed" is used in this thesis to denote a poorly permeable bed within a relatively permeable aquifer. Such interbeds are assumed to be as follows: (1) of significantly lower hydraulic conductivity than the surrounding sediments considered to be aquifer material yet porous and permeable enough to accept or release water in response to head changes in adjacent aquifer material; (2) of insufficient lateral extent to be considered a confining bed that separates adjacent aquifers; (3) of relatively small thickness in comparison to lateral extent. The interbedded sands have relatively less resistance to vertical flow than do the clays.

The interbed storage coefficient is a function of the mechanical properties of the compressible material and the thickness of the beds. (In this study, the sand fraction is proportional to the interbed storage coefficient.) The land subsidence model is based on Terzaghi's (1925) effective stress principle. Effective stress,  $p'$ , is expressed as the difference between total stress,  $p$ , and fluid pressure,  $u$ ,

$$p' = p - u \quad (3-2)$$

A change in head by discharging in the aquifer causes a change in effective stress, which causes the compressible materials to expand or compact, as shown in equation (3-3) (Poland and Davis, 1969),

$$\Delta p' = -r_w \Delta h \quad (3-3)$$

where  $\Delta h$  is change in head in a confined aquifer, positive for increase a negative for decrease in head and  $r_w$  is the unit weight of water.

Elastic compaction or expansion of sediments is proportional to the change in effective stress, expressed as

$$\Delta b = \frac{\Delta p'}{r_w} S_{ske} b_o \quad (3-4)$$

where  $\Delta b$  is change in thickness,  $S_{ske}$  is elastic specific storage, and  $b_o$  is the thickness of the interbed (Riley, 1969; Helm, 1975).

For sediments in confined aquifers where geostatic pressure is constant, the relation between change in head and change in thickness is (Leake and Prudic 1991)

$$\Delta b = -\Delta h S_{ske} b_o. \quad (3-5)$$

Also, inelastic compaction can be expressed as (Leake and Prudic 1991)

$$\Delta b^* = \frac{\Delta p'}{r_w} S_{skv} b_o, \quad (3-6)$$

$$\Delta b^* = -\Delta h S_{skv} b_o, \quad (3-7)$$

where  $\Delta b^*$  is inelastic compaction, and  $S_{skv}$  is the inelastic specific storage.

#### Incorporating Storage Changes into the Ground Water Flow Model

The ground water flow equation, equation (3-1), can be expressed as:

$$\frac{\partial}{\partial x} \left( K_{xx} \frac{\partial h}{\partial x} \right) + \frac{\partial}{\partial y} \left( K_{yy} \frac{\partial h}{\partial y} \right) + \frac{\partial}{\partial z} \left( K_{zz} \frac{\partial h}{\partial z} \right) - W = S_s \frac{\partial h}{\partial t}, \quad (3-8)$$

where  $x$ ,  $y$ , and  $z$  are cartesian coordinates;  $K_{xx}$ ,  $K_{yy}$ , and  $K_{zz}$  are principal components of the hydraulic conductivity tensor;  $h$  is hydraulic head;  $W$  is volumetric flux per unit volume of sources and sinks of water;  $S_s$  is specific storage of aquifer material; and  $t$  is time (McDonald and Harbaugh, 1988).

Assume head changes result in effective stress changes. To account for changes in storage caused by compaction of interbeds, an additional term has been added to the ground water flow equation,

$$\frac{\partial}{\partial x} \left( K_{xx} \frac{\partial h}{\partial x} \right) + \frac{\partial}{\partial y} \left( K_{yy} \frac{\partial h}{\partial y} \right) + \frac{\partial}{\partial z} \left( K_{zz} \frac{\partial h}{\partial z} \right) - W = S_s \frac{\partial h}{\partial t} + q_i, \quad (3-9)$$

and

$$q_i = S'_{sk} \frac{\partial h}{\partial t}, \quad (3-10)$$

where  $q_i$  is rate of flow per unit volume of water flowing into storage in compressible interbeds, and  $S'_{sk}$  is specific storage of interbeds.

The finite-difference expression of the implicit methods of  $q_i$  is

$$q_i^m = \frac{S_{sk}^m}{\Delta t} (h^m - H^{m-1}) + \frac{S_{ske}^m}{\Delta t} (H^{m-1} - h^{m-1}), \quad (3-11)$$

where  $S_{sk}^m = S_{ske}$ ,  $h^m > H^{m-1}$ ,  
 $S_{sk}^m = S_{skv}$ ,  $h^m \leq H^{m-1}$ , and

$m$  is the  $m$ -th time step (Leake and Prudic, 1991).

Compaction during a time step can be computed by multiplying equation (3-11) by the time step,  $\Delta t$ , and by interbed thickness,  $b_o$ . The rearranged equation (3-11) is equivalent to the sum of elastic and inelastic compaction in equations (3-5) and (3-7). In other words, the total compaction can be computed from equation (3-11).

### Parameters in the Model

The parameters used in the model are listed in Table 3-1. The sources or the methods to obtain parameters are also shown in the table.

The methods used to estimate the parameters in Table 3-1 and to obtain simulation results are as follows:

- (1) Model the Houston-Galveston region as a four-layer gridded water-winter system. Each layer in the model has thirty columns and thirty rows. Each element in the Houston-Galveston regional model has a dimension: 2.5 miles by 2.5 miles by 500 feet. Two points are used to locate the grid. The upper-left corner is located on the



Table 3-1 Sources and Methods to Obtain Parameters

Parameters	Sources	Methods
aquifer elevations	U.S.G.S.	mapping (transfer and rotation)
hydraulic conductivity	U.S.G.S.	digitization
hydraulic head	U.S.G.S.	digitization
sand fraction	B.E.G.	digitization
storage coefficient (of confined layer) or specific yield (of unconfined layer)	U.S.G.S.	digitization
transmissivity	U.S.G.S.	digitization
vertical elastic storage coefficient	U.S.G.S. and Bravo's work	soil log analysis and stochastic regeneration
vertical inelastic storage coefficient	U.S.G.S. and Bravo's work	soil log analysis and stochastic regeneration
vertical hydraulic conductivity	U.S.G.S. and Bravo's work	soil log analysis and stochastic regeneration
well location and discharge rate	Harris-Galveston Coastal Subsidence District	mapping

Procedures

The methods used to estimate the parameters in Table 3-1 and to obtain simulation results are as follows:

- (1) Model the Houston-Galveston region as a four-layer ground water aquifer system.

Each layer in the model has thirty columns and thirty rows. Each element in the Houston-Galveston regional model has a dimension: 2.5 miles by 2.5 miles by 500 feet. Two points are used to locate the grid. The upper-left corner is located on the

border of Harris, Ft. Bend, and Waller counties. The lower-right corner is located on Galveston Bay (Figure 3-3).

(2) Digitize sand fraction of the grid.

By using maps from Kreitler (1977), the distribution of sand fraction of most elements are digitized and fit into the ground water flow model.

(3) Generate missing sand fraction data.

Geological maps from Kreitler (1977) do not provide all the sand fraction data in the model. About 300 of 900 elements of sand fraction data in each layer were missing. Using random sampling and stochastic regeneration methods, those missing data are regenerated. ( The details of random & stochastic methods are described in Chapter 5)

(4) Generate vertical geological data of the grid.

Vertical hydraulic conductivity ( $K_z$ ), vertical elastic storage coefficient ( $S_{ske}$ ), and vertical inelastic storage coefficient ( $S_{skv}$ ) are three parameters. Based on Bravo's theory, geological data of three logs are used to determine  $K_z$ ,  $S_{ske}$ ,  $S_{skv}$ . The locations of the logs are at Baytown, Clear Lake, and the Southwest area. The geological characteristics of three logs are listed in Chapter 5. By using statistical correlation methods, a relationship between sand fraction and vertical geological parameters ( $K_z$ ,  $S_{ske}$ ,  $S_{skv}$ ) was computed. The vertical geological  $K_z$ ,  $S_{skv}$ , and  $S_{ske}$  in the grid are generated from this relationship.

(5) Substitute horizontal hydrogeologic data into the model.

Hydrogeologic parameters include transmissivity, hydraulic conductivity, and storage coefficient. U.S.G.S. maps were used to estimate these parameters on the grid.

(6) Find ground water pumpage.

Figure 3-3 Location of Modelling Area

The ground water pumping data, which includes locations, screen depths, and the discharge rates of the wells, were obtained from the Harris-Galveston Coastal

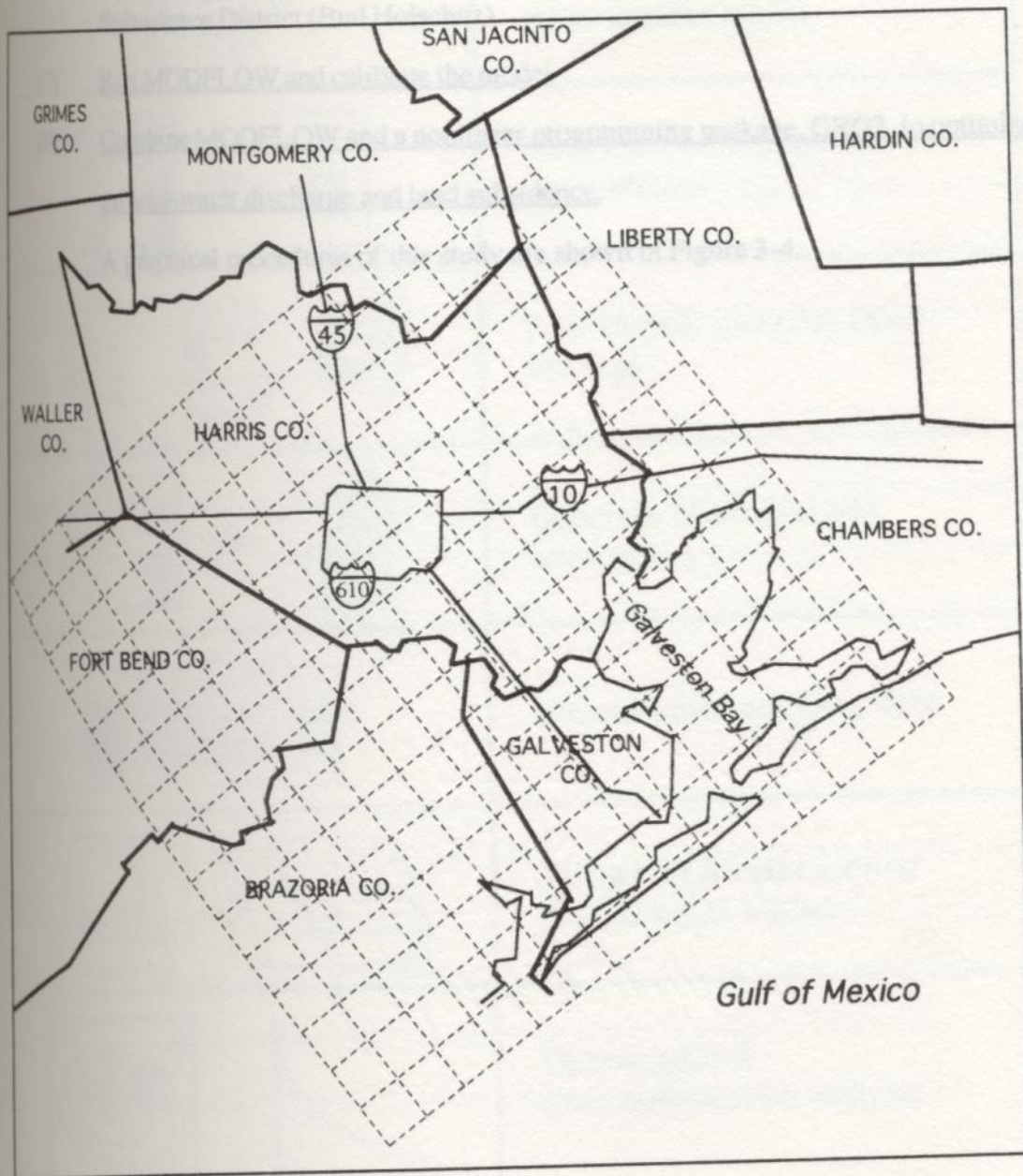


Figure 3-3 Locations of Modelling Area

The ground water pumping data, which includes locations, screen depths, and the discharge rates of the wells, were obtained from the Harris-Galveston Coastal Subsidence District (Bud Holschuz).

- (7) Run MODFLOW and calibrate the model.
- (8) Combine MODFLOW and a nonlinear programming package, GRG2, to optimize ground-water discharge and land subsidence.

A graphical procedures of this study are shown in Figure 3-4.

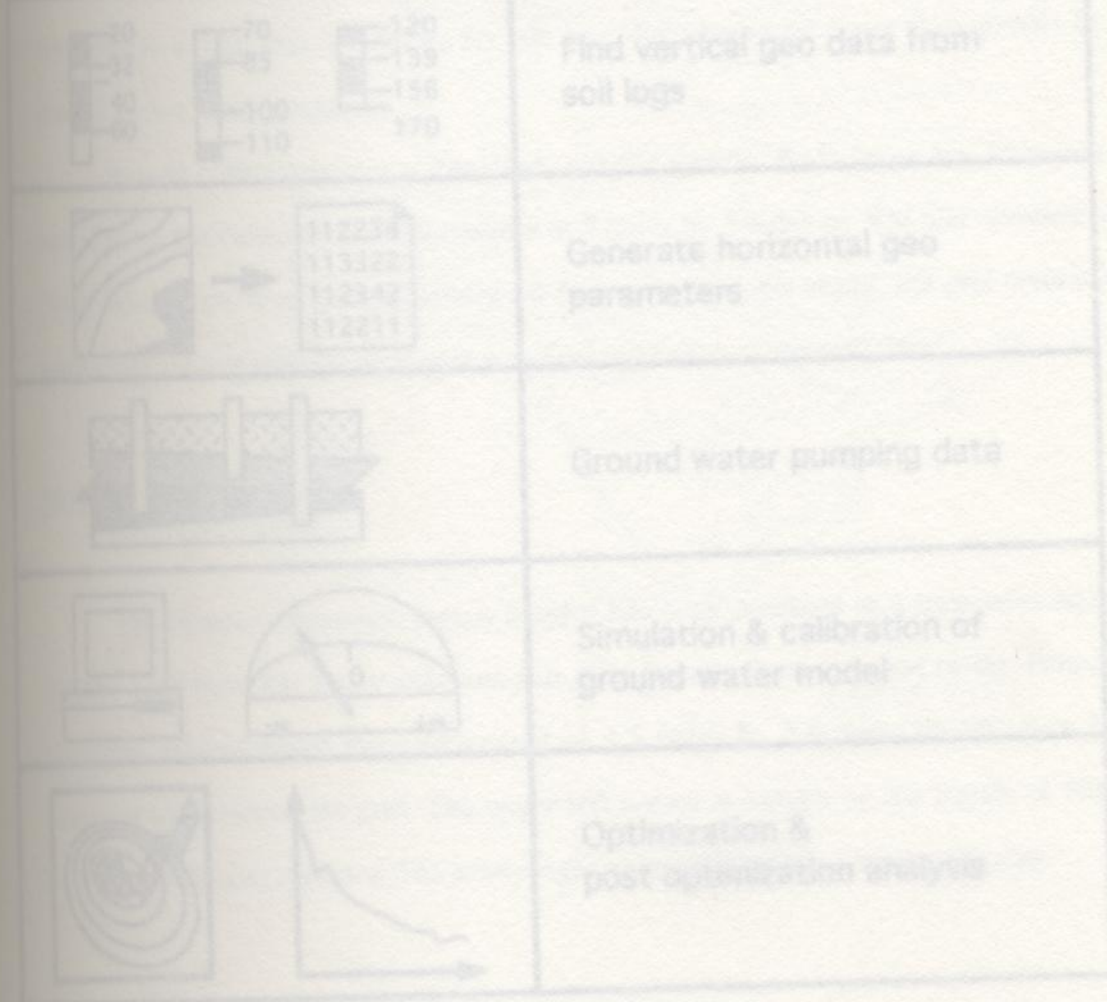
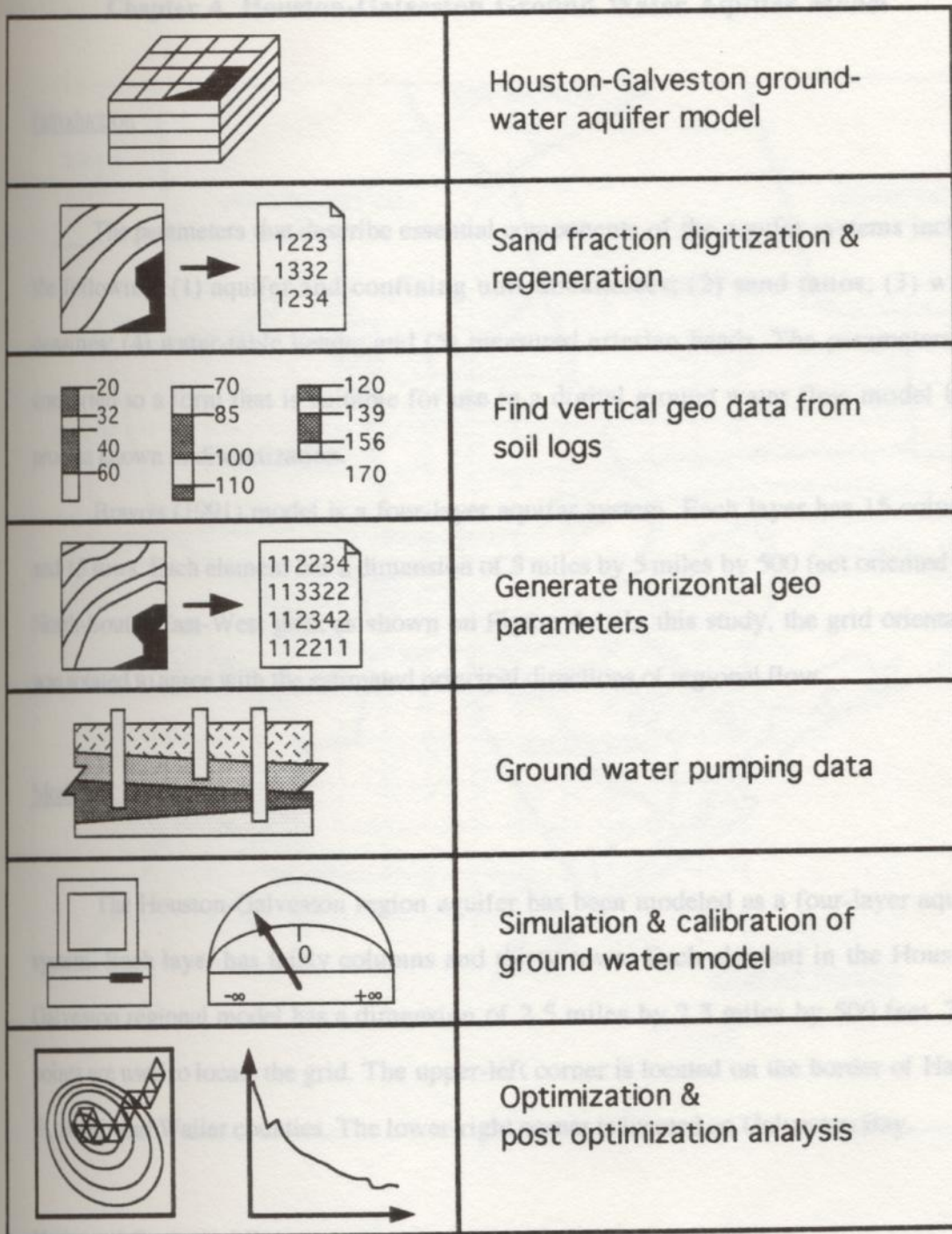


Figure 3-4 Flowchart



The data of transmissivities, hydraulic conductivities, storage coefficients, heads, and layer elevations are from U.S. Geological Survey (2 and 4-3)

Figure 3-4 Flowchart

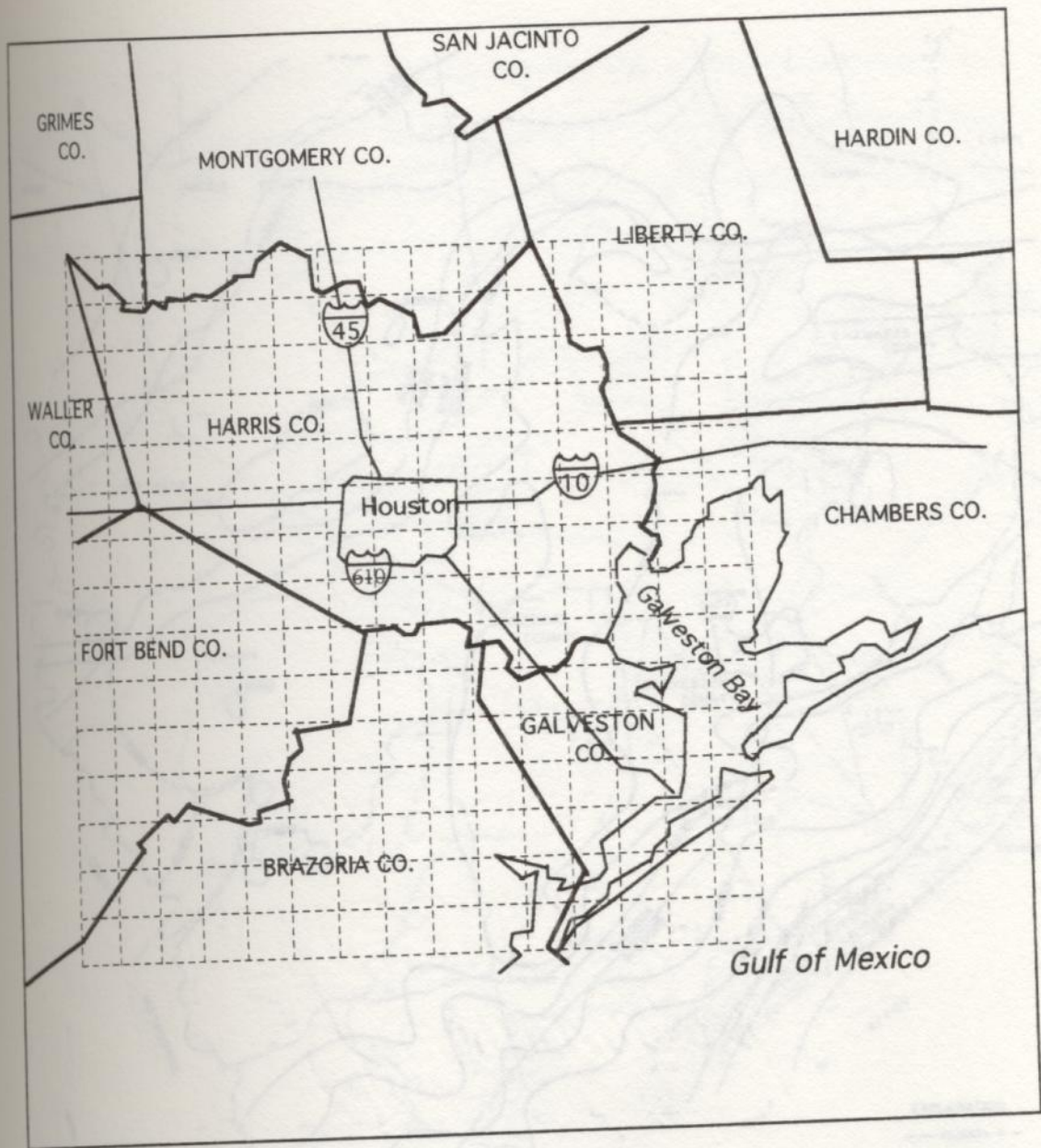
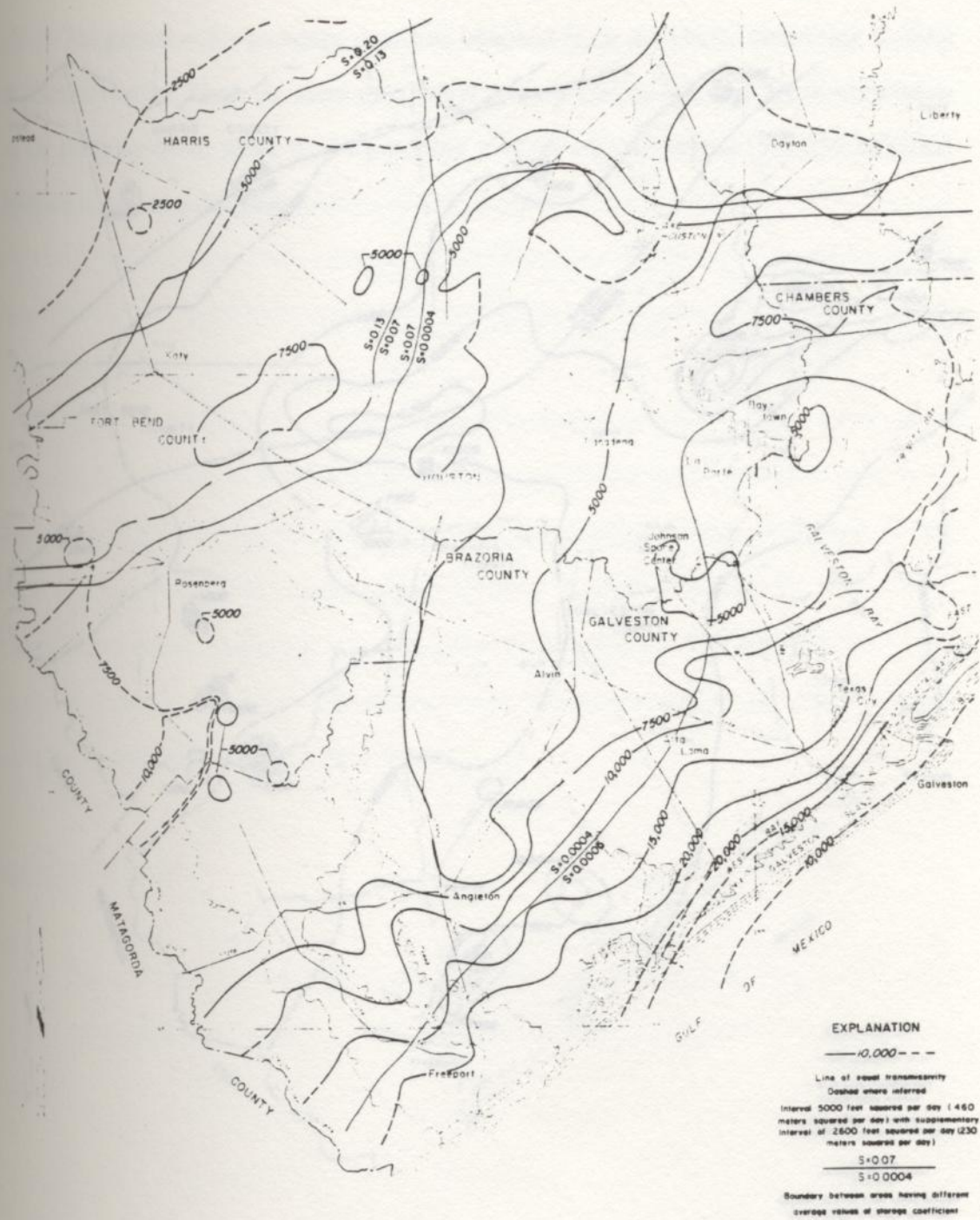


Figure 4-1 Locations of Bravo's Modeling Area (Bravo, 1990)



**EXPLANATION**

- 10,000 — —
- Line of equal transmissivity  
Dashed where referred
- Interval 5000 feet squared per day (460  
meters squared per day) with supplementary  
interval of 2600 feet squared per day (230  
meters squared per day)
- 0.07 — —
- 0.0004 — —
- Boundary between areas having different  
average values of storage coefficient

Figure 4-2 Estimated transmissivity and storage coefficient of the Chicot aquifer (Jorgensen, 1975)

Ground Water Pumpage

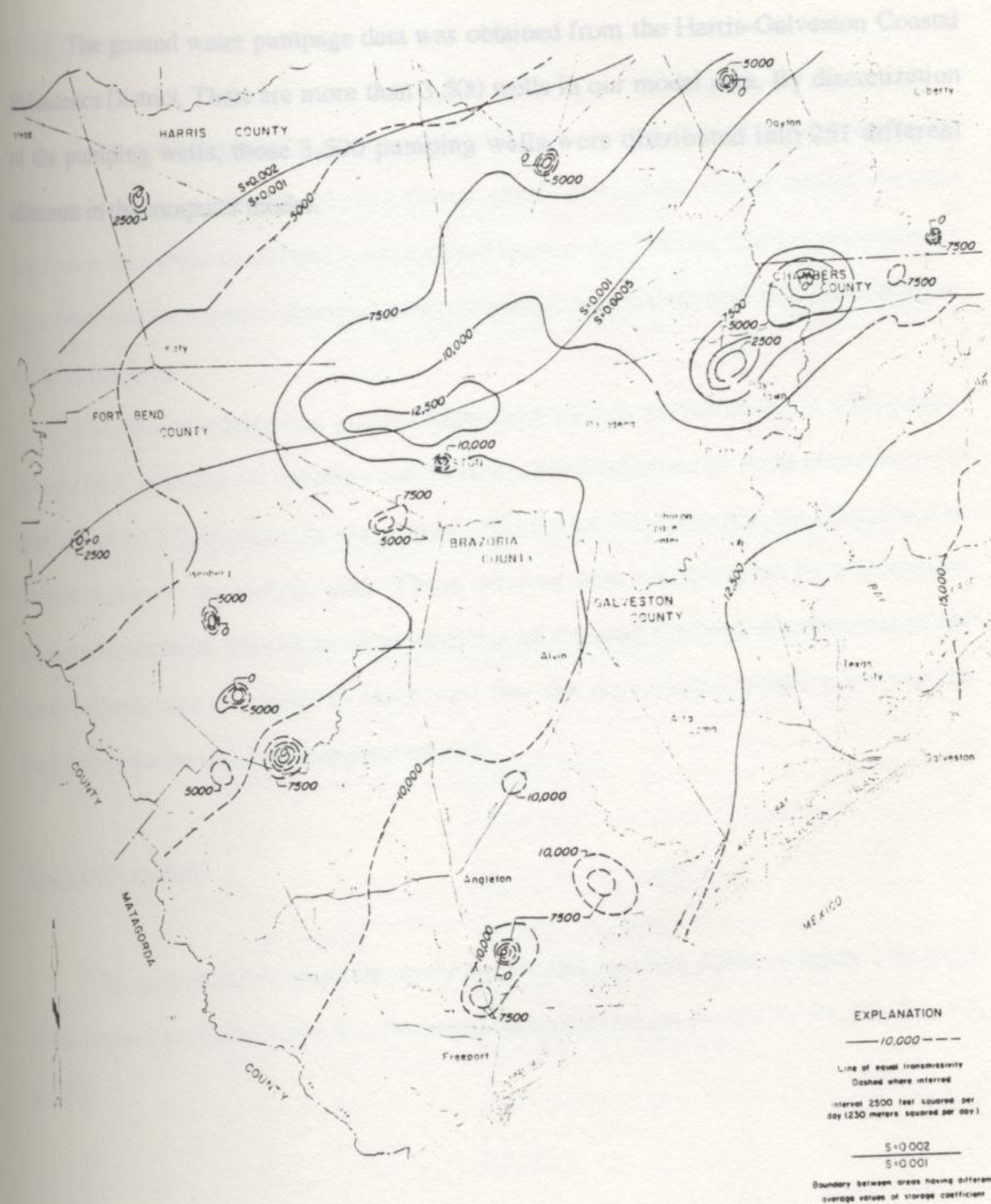


Figure 4-3 Estimated transmissivity and storage coefficient of the Evangeline aquifer (Jorgensen, 1975)



The ground water pumpage data was obtained from the Harris-Galveston Coastal Subsidence District. There are more than 3,500 wells in our model area. By discretization of the pumping wells, those 3,500 pumping wells were distributed into 251 different elements in the computer model.

The sand fractions of the aquifer model had to be digitized from maps. Drilling and geophysical logs from three sites were used to determine the relationship between interbed storage coefficient and sand fractions.

The Houston-Galveston ground water flow model, in this study, is a four-layer system. Each layer has 30 columns and 30 rows. Sand fractions of most elements were digitized from B.E.G. maps. In every layer, 300 out of 900 elements' sand fraction data are not shown on the B.E.G. map. Those missing data are recreated by a stochastic regeneration method. Statistical characteristics of the sand fraction distributions of the aquifer system are computed to make sure that the regenerated model preserves the statistical characteristics of the original dataset.

### Sand Fraction Type

The sand fraction data in the study are divided into five different types. The range of each type is shown in Table 5-1. Five sand fraction types are named as P1, P2, P3, P4, and P5.

## Chapter 5 Interbed Storage Coefficients

### Introduction

In this study, interbed storage coefficients are assumed to be proportional to sand fractions. In order to compute interbed storage coefficients of the aquifer model, the sand fractions of the aquifer model had to be digitized from maps. Drilling and geophysical logs from three sites were used to determine the relationship between interbed storage coefficient and sand fractions.

The Houston-Galveston ground water flow model, in this study, is a four-layer system. Each layer has 30 columns and 30 rows. Sand fractions of most elements were digitized from B.E.G. maps. In every layer, 300 out of 900 elements' sand fraction data are not shown on the B.E.G. map. Those missing data are recreated by a stochastic regeneration method. Statistical characteristics of the sand fraction distributions of the aquifer system are computed to make sure that the regenerated model preserves the statistical characteristics of the original dataset.

### Sand Fraction Type

The sand fraction data in the study are divided into five different types. The range of each type is shown in Table 5-1. Five sand fraction types are named as F1, F2, F3, F4, and F5.

Table 5-1 Range of the Sand Fraction

Sand Fraction Type	Range of Type
F1	sand fraction less than 30%
F2	sand fraction between 30-40%
F3	sand fraction between 40-50%
F4	sand fraction between 50-60%
F5	sand fraction higher than 60%

Element Type

The elements in the model can be divided into three types, as shown in Table 5-2.

Table 5-2 Three Types of Elements

Element Type	Status	Explanation
A	known	The sand fraction of the cell can be digitized from B.E.G. maps.
B	intermediate	The sand fraction of the element is not on maps, but the element is beside one or several know elements.
C	unknown	The sand fraction of the element is not on maps.

## Regeneration Methods

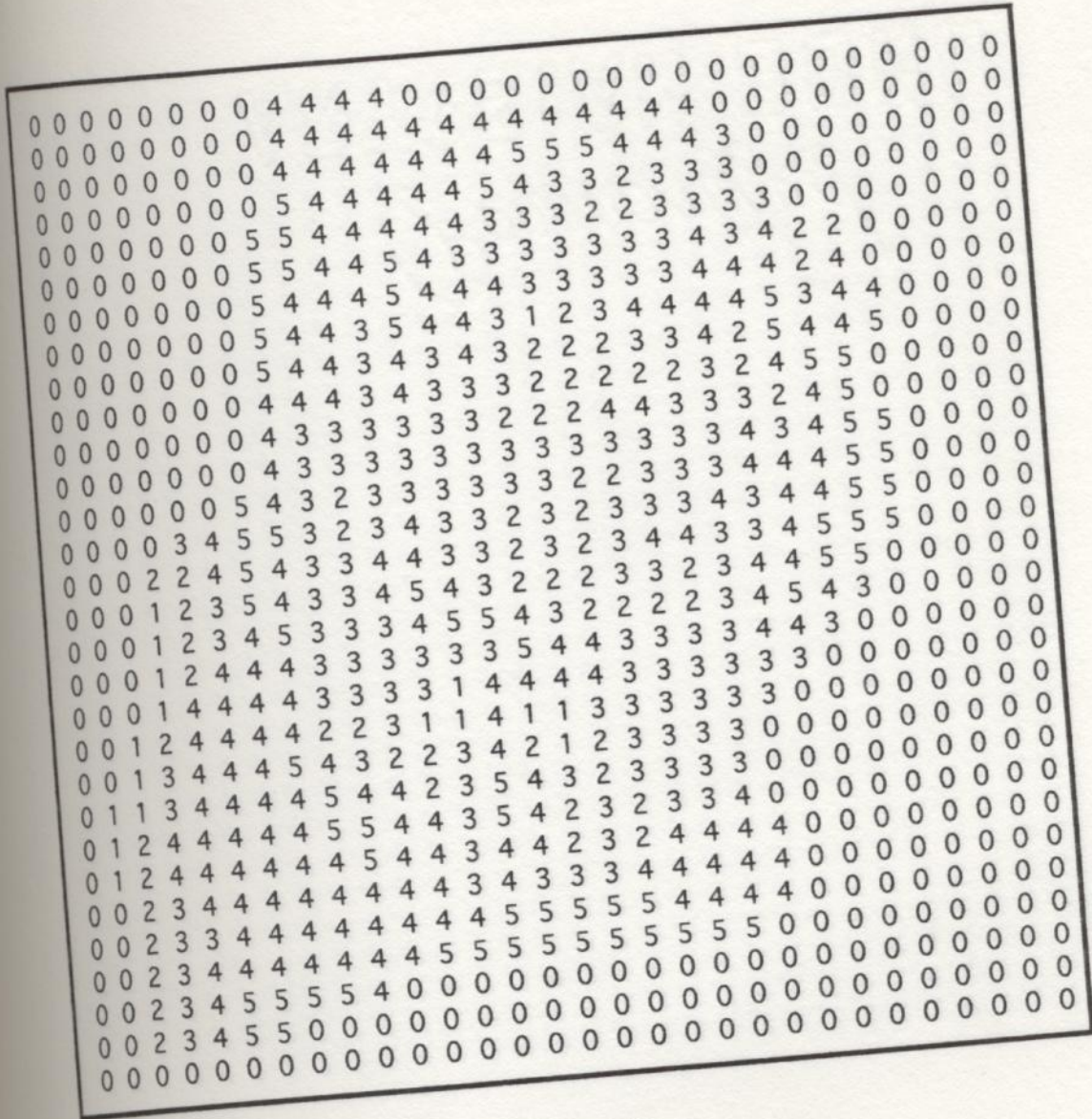
Three methods were used to generate missing sand fraction data:

- (1) Kriging using a graphic software package - Surfer (SURFER 1990).
- (2) Linear interpolation using a graphic software package - Spyglass (Spyglass 1990).
- (3) Stochastic regeneration method (details in the next section).

The last method were a regenerated sand fraction that preserved the properties of the original data better than other methods. The sand fraction maps of the original map and three method maps are shown in Figures 5-1, 5-2, 5-3, and 5-4. Large areas of high sand fraction and low sand fraction were observed from regenerated sand fraction maps of Kriging method and linear interpolation method (Figures 5-3 and 5-4). It is not consistent with the original sand fraction map (Figure 5-1). A comparison of four sand fraction maps in the first layer of the model is shown in Table 5-3. In the table, P(F1), P(F2), P(F3), P(F4), and P(F5) represent the appearance percentages of the F1, F2, F3, F4, and F5 in the maps, respectively (F1, F2, F3, F4, and F5 were defined in Table 5-1). The stochastic method provided a closer regenerated sand fraction map to the original map than the other two methods.

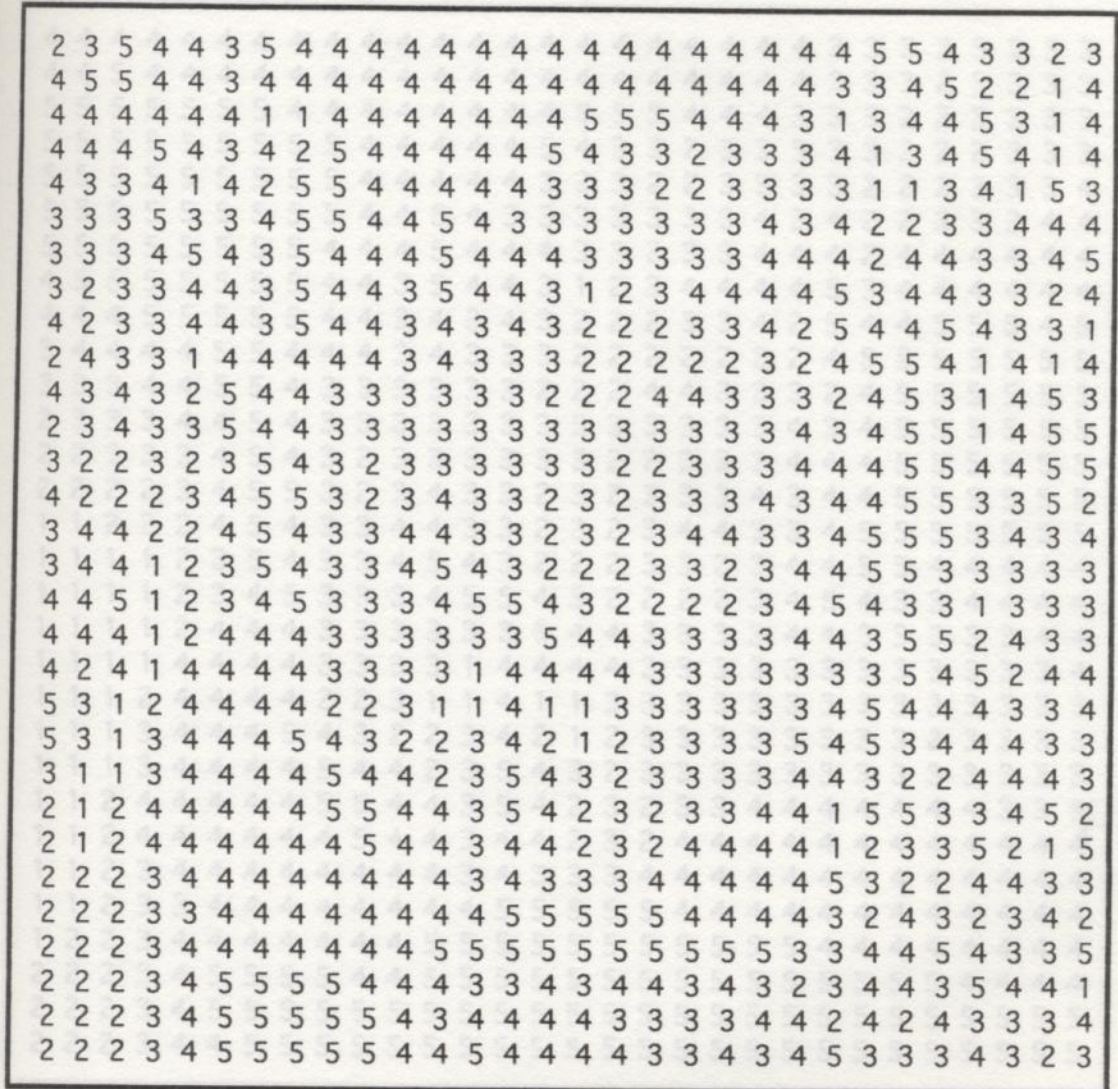
Table 5-3 A Comparison of Sand Fraction Appearance Percentage

	P(F1)	P(F2)	P(F3)	P(F4)	P(F5)
Original	0.03314	0.12086	0.31969	0.38791	0.13840
Stochastic	0.04333	0.12556	0.31222	0.38333	0.13556
Kriging	0.04778	0.09778	0.27222	0.34333	0.23889
Linear	0.12222	0.10667	0.21333	0.27222	0.28556



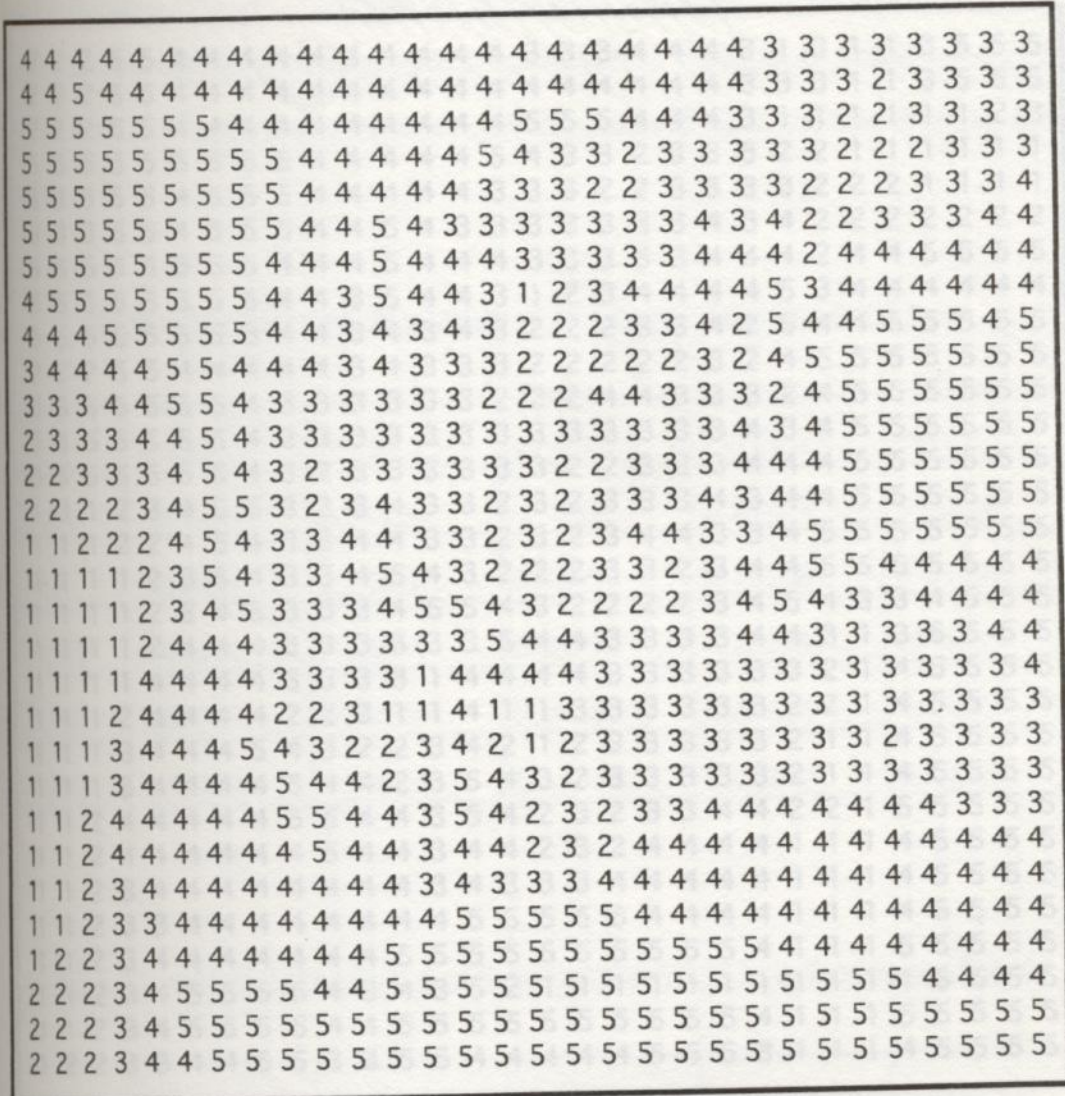
- 0 Elements without sand fraction data
- 1 Elements with sand fraction less than 30%
- 2 Elements with sand fraction between 30% and 40%
- 3 Elements with sand fraction between 40% and 50%
- 4 Elements with sand fraction between 50% and 60%
- 5 Elements with sand fraction higher than 60%

Figure 5-1 Original Sand Fraction Distribution map of the First Layer



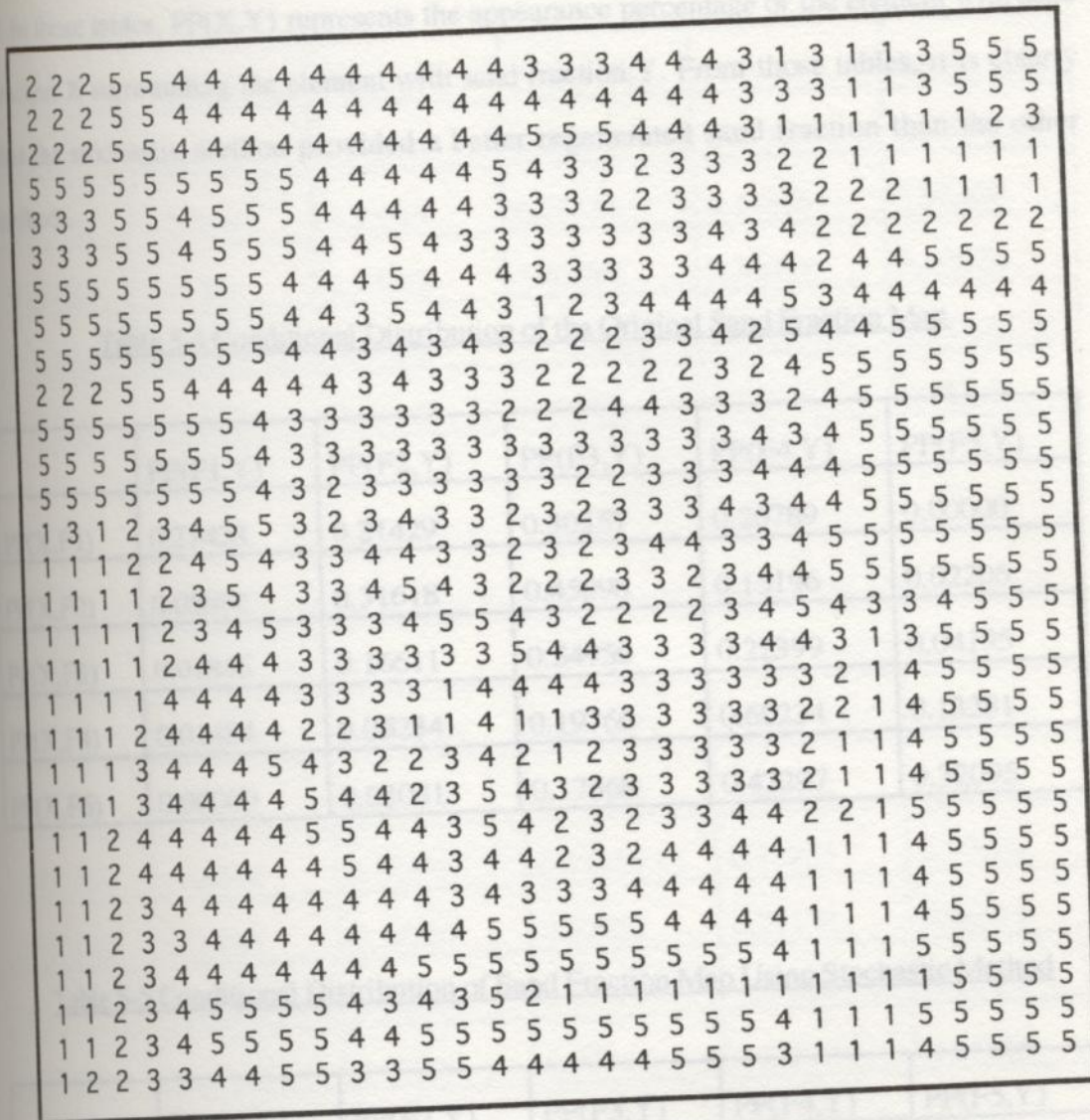
- 0 Elements without sand fraction data
- 1 Elements with sand fraction less than 30%
- 2 Elements with sand fraction between 30% and 40%
- 3 Elements with sand fraction between 40% and 50%
- 4 Elements with sand fraction between 50% and 60%
- 5 Elements with sand fraction higher than 60%

Figure 5-2 Stochastic Regenerated Sand Fraction Map of the First Layer



- 0 Elements without sand fraction data
- 1 Elements with sand fraction less than 30%
- 2 Elements with sand fraction between 30% and 40%
- 3 Elements with sand fraction between 40% and 50%
- 4 Elements with sand fraction between 50% and 60%
- 5 Elements with sand fraction higher than 60%

Figure 5-3 Kriging Regenerated Sand Fraction Map of the First Layer



- 0 Elements without sand fraction data
- 1 Elements with sand fraction less than 30%
- 2 Elements with sand fraction between 30% and 40%
- 3 Elements with sand fraction between 40% and 50%
- 4 Elements with sand fraction between 50% and 60%
- 5 Elements with sand fraction higher than 60%

Figure 5-4 Linear Interpolation Regenerated Sand Fraction Map of the First Layer



A comparison of conditional distributions is shown in Tables 5-4, 5-5, 5-6, and 5-7. In those tables,  $PP(X,Y)$  represents the appearance percentage of the element with sand fraction  $X$  surrounding the element with sand fraction  $Y$ . From those tables, it is clearly that the stochastic method provided a better regenerated sand fraction than the other methods.

Table 5-4 Conditional Distribution of the Original Sand Fraction Map

	PP(F1,Y)	PP(F2,Y)	PP(F3,Y)	PP(F4,Y)	PP(F5,Y)
PP(X,F1)	0.21428	0.21429	0.30357	0.26789	0.00000
PP(X,F2)	0.05882	0.31618	0.45098	0.15196	0.02206
PP(X,F3)	0.01846	0.16611	0.54950	0.22399	0.04195
PP(X,F4)	0.01484	0.05234	0.19766	0.60234	0.13281
PP(X,F5)	0.00000	0.03041	0.17568	0.47297	0.32095

Table 5-5 Conditional Distribution of Sand Fraction Map Using Stochastic Method

	PP(F1,Y)	PP(F2,Y)	PP(F3,Y)	PP(F4,Y)	PP(F5,Y)
PP(X,F1)	0.19257	0.18581	0.25000	0.29730	0.07432
PP(X,F2)	0.06316	0.32895	0.37632	0.18026	0.05132
PP(X,F3)	0.03472	0.13889	0.48909	0.25992	0.07738
PP(X,F4)	0.03421	0.05532	0.21706	0.54899	0.14443
PP(X,F5)	0.02404	0.04808	0.18269	0.40505	0.34014

Table 5-6 Conditional Distribution of Sand Fraction Map Using Kriging Method

	PP(F1,Y)	PP(F2,Y)	PP(F3,Y)	PP(F4,Y)	PP(F5,Y)
PP(X,F1)	0.62917	0.20000	0.09167	0.07917	0.00000
PP(X,F2)	0.07969	0.39219	0.39531	0.11875	0.01406
PP(X,F3)	0.01211	0.13932	0.61784	0.20099	0.02974
PP(X,F4)	0.00883	0.03532	0.16822	0.63801	0.14963
PP(X,F5)	0.00000	0.00632	0.03792	0.23034	0.72542

Table 5-7 Conditional Distribution of Sand Fraction Map Using Linear Interpolation

	PP(F1,Y)	PP(F2,Y)	PP(F3,Y)	PP(F4,Y)	PP(F5,Y)
PP(X,F1)	0.61176	0.14853	0.07059	0.08824	0.08088
PP(X,F2)	0.14368	0.33477	0.32328	0.11925	0.07902
PP(X,F3)	0.03581	0.15730	0.53020	0.21138	0.06531
PP(X,F4)	0.03363	0.04652	0.17769	0.56334	0.17881
PP(X,F5)	0.03377	0.03199	0.05746	0.20024	0.67654

A large sample Z-test was used to test the sand fraction maps from three methods (Mendenhall, etc. 1986). Several estimators,  $\theta_1$ ,  $\theta_2$ ,  $\theta_3$ ,  $\sigma_\theta$ , and  $Z$ , were computed in order to conduct the Z-test, where

$$\theta_1 = \sum \frac{x}{n},$$

$$\theta_2 = \sum \frac{x^2}{n},$$

$$\theta_3 = \sum \frac{x^3}{n},$$

$$\sigma_{\theta_i} = \frac{\sum (x - \theta_i)^2}{n}, \quad i=1, 2, \text{ or } 3, \text{ and}$$

$$Z_i = \frac{\theta_{i_j} - \hat{\theta}_{i_{original}}}{\sqrt{\sigma_{\theta_{i_j}}^2}}, \quad i=1, 2, \text{ or } 3, \text{ and } j= 1, 2, \text{ or } 3.$$

(1) The Z-test results are shown in Table 5-8. P-value results are shown in Table 5-9.

Table 5-8 Results of the Z-test

	Stochastic Method	Kriging Method	Linear Method
Z <sub>1</sub>	-0.0348	0.1374	0.0110
Z <sub>2</sub>	-0.0192	0.1199	0.0855
Z <sub>3</sub>	-0.0169	0.1463	0.1435

Table 5-9 The p-value

	Stochastic	Kriging Method	Linear Method
P1	0.972	0.888	0.992
P2	0.984	0.904	0.932
P3	0.988	0.881	0.888

The p-values for all three methods are very large indicating that all methods produce data sets whose estimators are not statistically different to the estimators from the original data. However, the stochastic method has slightly better performance in the higher order estimates. Because preserving higher order estimates is considered important in this study, the stochastic method was chosen to regenerate the sand fraction map.

## Stochastic Regeneration Method

Procedures of the stochastic regeneration method used in this study are described in this section. Also, a graphical flowchart of the stochastic regeneration method is shown in Figure 5-5.

- (1) Use linear interpolation to determine sand fractions of type B elements.
- (2) From the original sand fraction map, the probability mass functions of sand fractions can be computed. Also, the conditional distribution of sand fractions surrounding a specific type element can be computed. These distributions are used for determining sand fractions of unknown elements.
- (3) Probability distributions of sand fractions are used as a weight function of a random generator. By using the random generator, random sand fraction values are assigned to 10% of unknown elements.
- (4) Probability mass functions for distributions of sand fractions surrounding a specific type element are used as weight functions of a random generator. By using the random generator, random sand fraction values are assigned to surrounding elements of a selected center element.
- (5) Use linear interpolation to fill the remaining unknown elements.

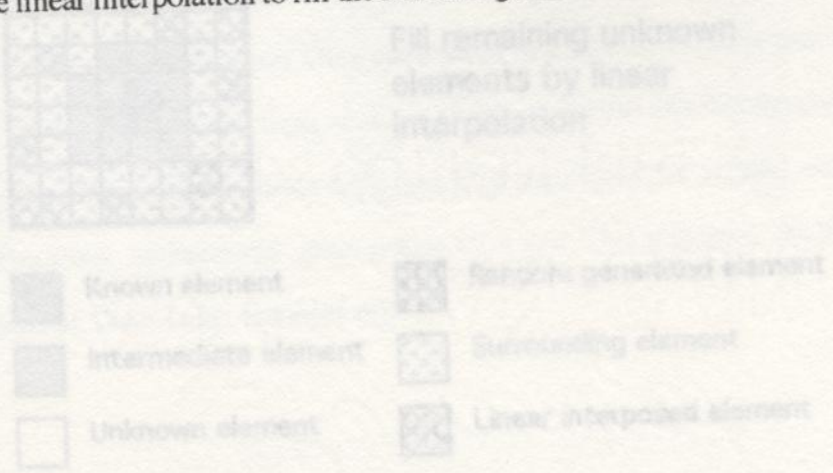
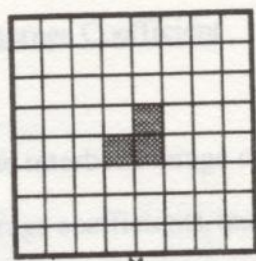
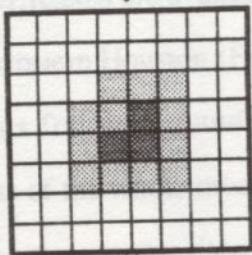


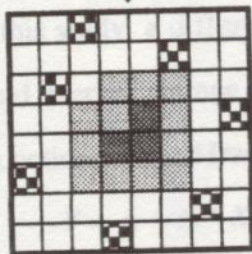
Figure 5-5 Flowchart of the Stochastic Regeneration Method



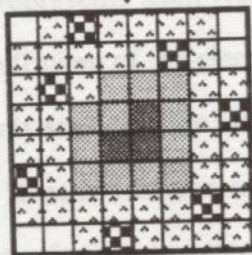
Original sand fraction distributions



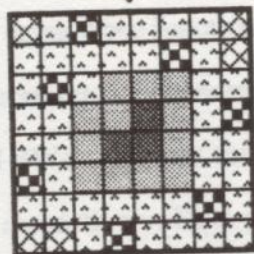
Compute sand fractions of intermediate elements by linear interpolation



Assign random sand fractions to selected elements



Assign sand fractions for surrounding elements (statistics and random method)



Fill remaining unknown elements by linear interpolation

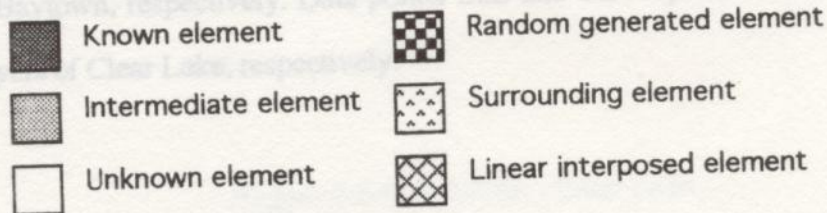


Figure 5-5 Flowchart of the Stochastic Regeneration Method

### Interbed Storage Coefficient

The interbed storage coefficients include vertical hydraulic conductivities, vertical elastic storage coefficients, and vertical inelastic storage coefficients. In this study, interbed storage coefficients are available only at three extensometer sites: Clear Lake, Baytown, and Southwestern Houston (Figures 5-6, 5-7, and 5-8). In order to have interbed storage coefficients for the ground water model, one can assume that the interbed storage coefficients of the whole model have the same value as the interbed storage coefficients from three extensometer sites (Bravo, 1990).

In this study, a different approach is used to find the relationship between sand fractions and interbed storage coefficients. The interbed storage coefficients are assumed to be linear functions of sand fraction,

$$Y = A + B * X ,$$

where  $X$  represents sand fraction of an aquifer model element,  $Y$  represents interbed storage coefficient of the element. If sand fraction is equal to 100%, the aquifer element contains only sand, and the interbed storage coefficient of the element is equal to a constant value,  $A$ . If sand fraction is 0%, the element is a pure clay aquifer. Once the linear functions are found, the interbed storage coefficients of the whole aquifer model can be computed using those functions. The sand fraction data and the interbed storage coefficient obtained from three extensometer sites are shown in Table 5-10. Data points SW1, SW2, SW3, and SW4 represent the first, second, third, and fourth aquifer layers of Southwest Houston, respectively. Data points BT2 and BT3 represent the second and third aquifer layers of Baytown, respectively. Data points CL3 and CL4 represent the third and fourth aquifer layers of Clear Lake, respectively.

Figure 5-6 Soil Profile - Clear Lake

Feet below  
land surface

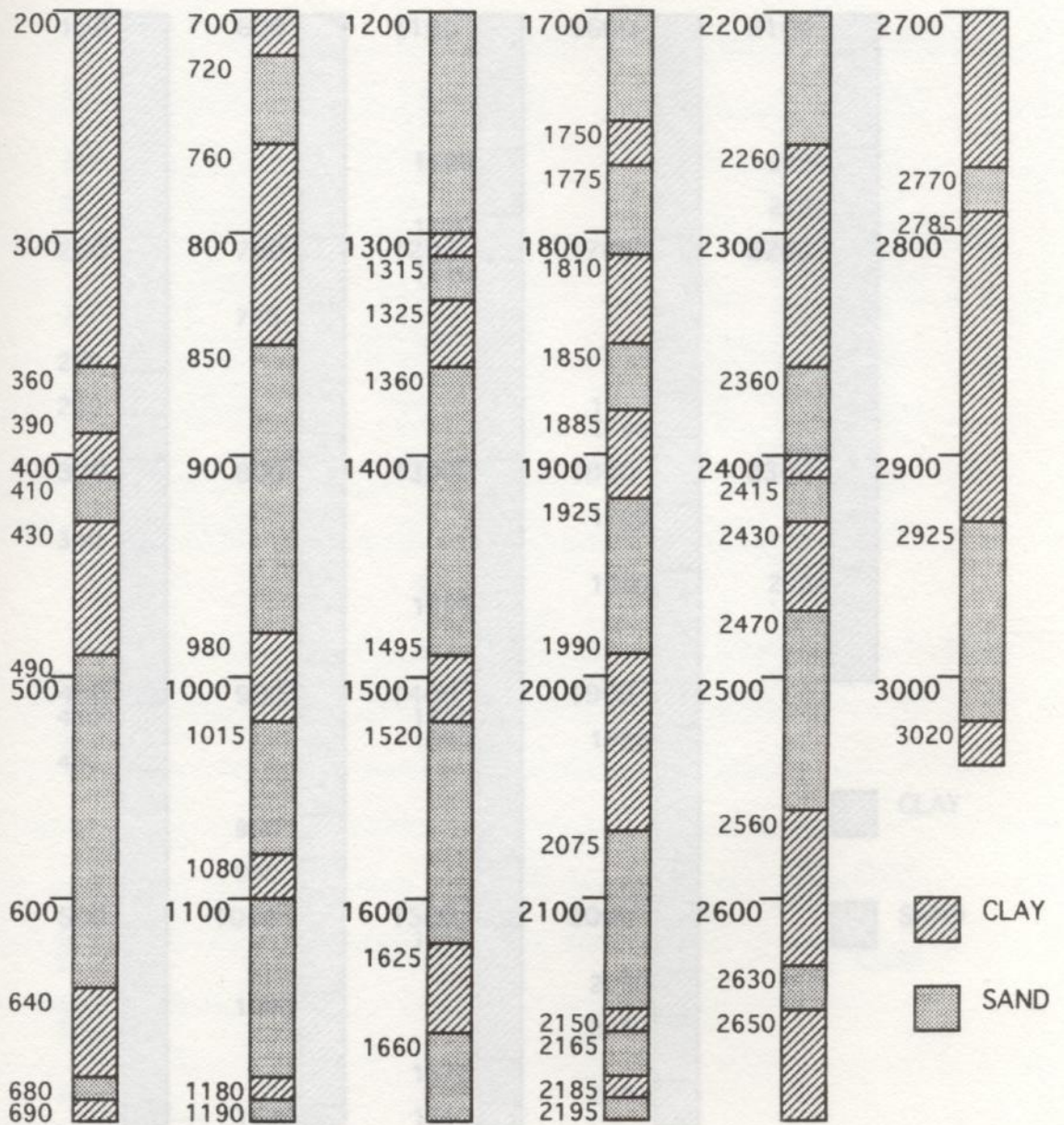


Figure 5-6 Soil Profile - Clear Lake

Feet below  
land surface

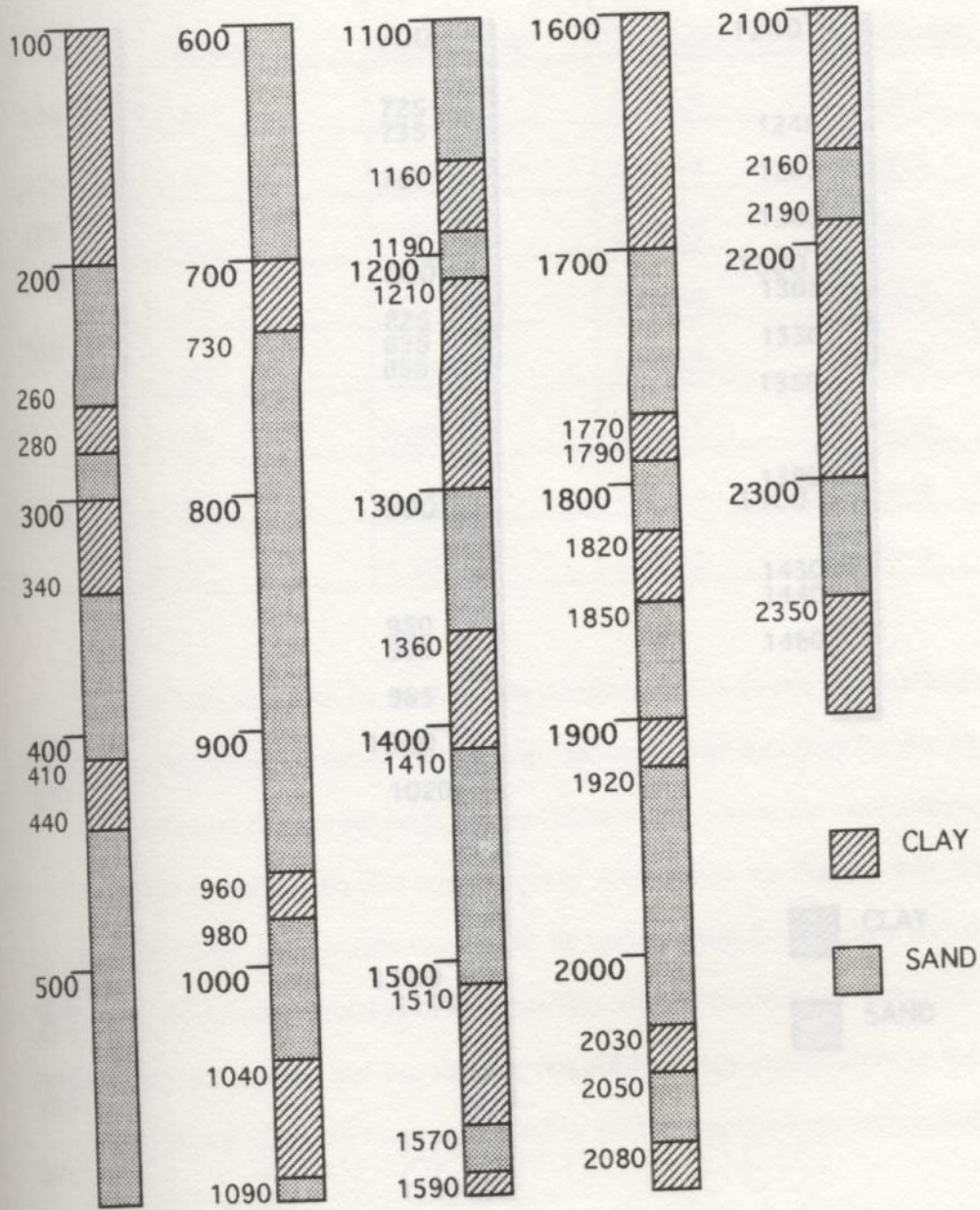


Figure 5-7 Soil Profile - Southwest Area



Table 5-10 Interbed Storage Coefficients Obtained from Extensometer Sites

	Sand Fraction	Hydraulic Conductivity	Elastic Storage Coefficient	Inelastic Storage Coefficient
SW1	0.525	5.10e-5	1.42e-5	4.70e-5
BT2	0.46	1.18e-4	2.75e-4	1.79e-3
SW2	0.90	3.96e-5	5.08e-5	6.20e-5
BT3	0.53	2.57e-4	2.75e-4	1.85e-3
CL3	0.80	1.18e-5	1.43e-5	1.71e-4
SW3	0.56	8.89e-5	2.30e-5	2.78e-5
CL4	0.67	9.88e-5	1.85e-4	5.60e-4
SW4	0.52	1.16e-5	2.26e-5	1.69e-4

By using a simple curve-fit method, the relationships between the interbed storage coefficients and sand fraction were found. Note that the linear function for the hydraulic conductivity was forced to pass the origin point (because the lower the sand fraction of an aquifer is, the lower the hydraulic conductivity should be). In Figure 5-9, the linear functions did not fit the data points very well. In fact, Figure 5-9 implies that the sand fraction may not be a linear function of the interbed storage coefficient. However, due to the limited extensometer data and unavailable interbed storage coefficients in the model, these linear functions (Figure 5-9) were still used to provide interbed storage coefficients of the computer aquifer model.

Figure 5-9 Relationship between Vertical Hydraulic Coefficients and Sand Fraction

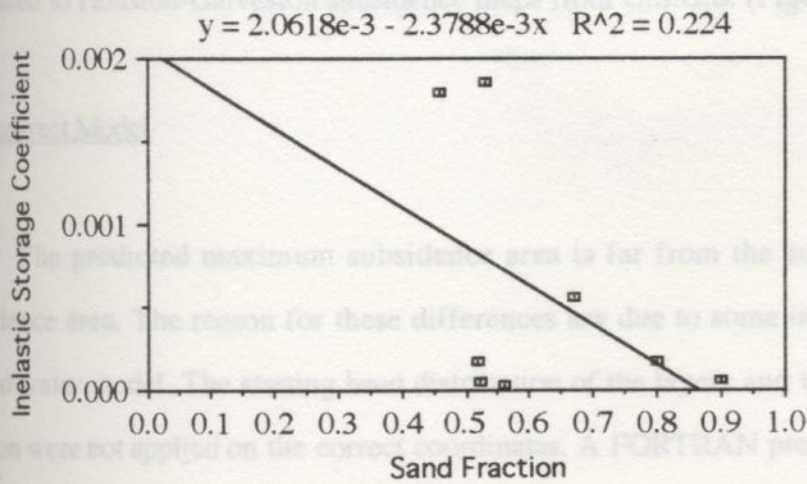
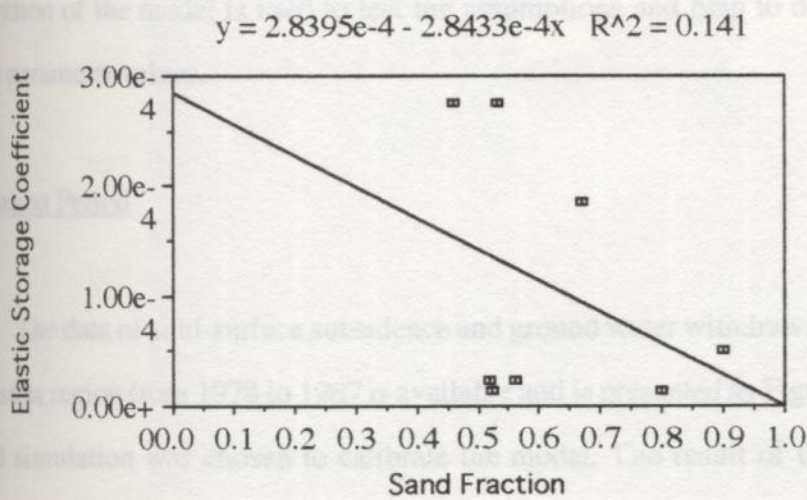
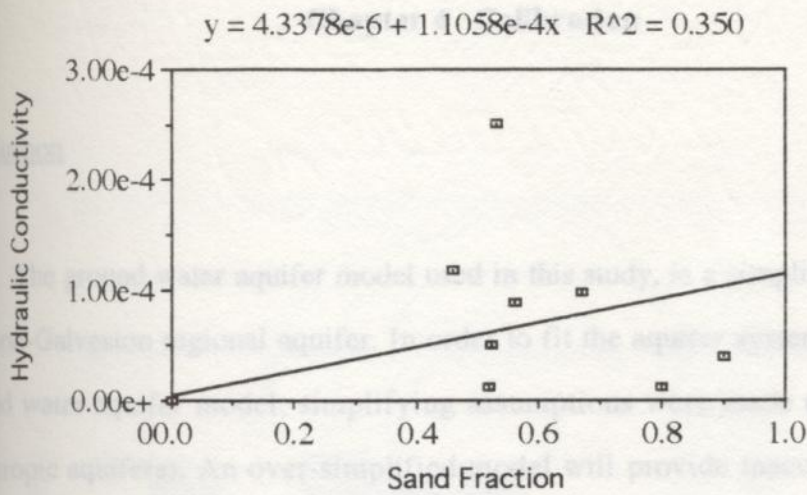


Figure 5-9 Relationship between Vertical Hydraulic Coefficients and Sand Fraction

## Chapter 6 Calibration

### Introduction

The ground water aquifer model used in this study, is a simplified system of the Houston-Galveston regional aquifer. In order to fit the aquifer system into a computer ground water aquifer model, simplifying assumptions were made (such as interbed, anisotropic aquifers). An over-simplified model will provide inaccurate predictions. Calibration of the model is used to test the assumptions and help to detect unreasonable model parameter values.

### Simulation Period

The data of land-surface subsidence and ground water withdrawals in the Houston-Galveston region from 1978 to 1987 is available and is presented as Figure 6-1. A ten-year period simulation was chosen to calibrate the model. The result of the simulation was compared to Houston-Galveston subsidence maps from U.S.G.S. (Figure 6-2).

### An Incorrect Model

The predicted maximum subsidence area is far from the surveyed maximum subsidence area. The reason for these differences are due to some incorrect data in the ground water model. The starting head distribution of the layers and the pumping wells' location were not applied on the correct coordinates. A FORTRAN program was coded to transfer Bravo's (1990) data into the model. The program didn't transfer the coordinates correctly.

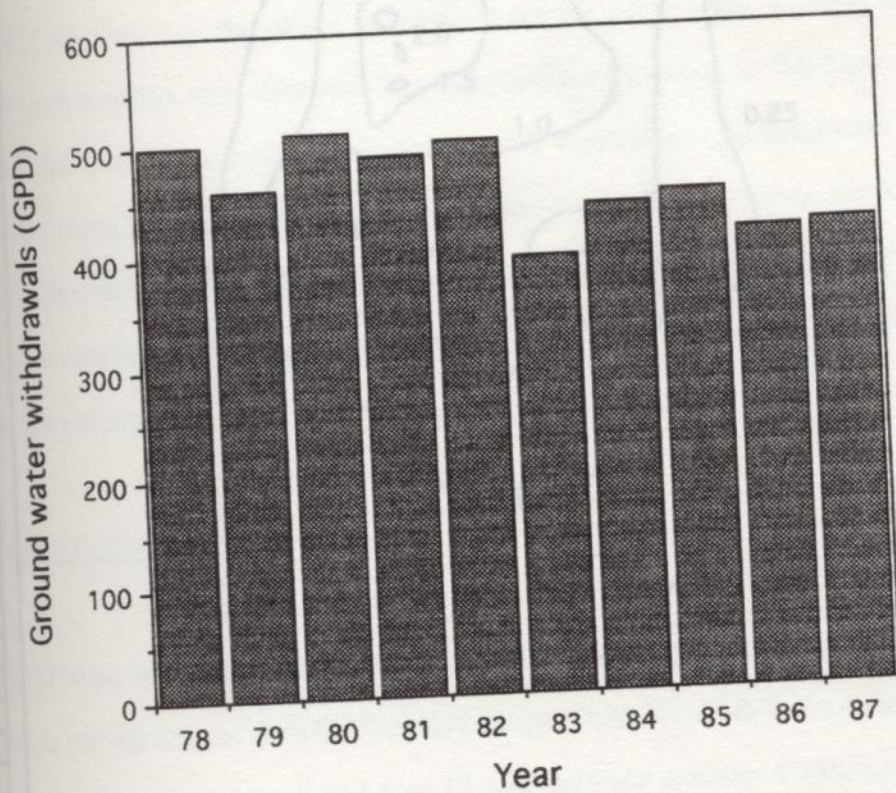


Figure 6-1 Ground Water Withdrawals in the Houston-Galveston Region, 1978-1987

Although the first calibration did not provide a reliable subsidence prediction, an interesting subsidence phenomena was found in this simulation. The maximum modeled subsidence did not occur in the location of the heavy ground water discharge, but rather, adjacent to these areas. Several factors may explain this result. The pre-developed head of the heavy pumping area was 100 feet lower than the pre-developed head of the nearby area; so much of the heavy ground water withdrawal did not come from the well location but from the surrounding area. Because the surrounding elements to the heavy pumping elements had much higher head drawdown in the simulation, the maximum subsidence occurred in these elements. Similar behavior was observed in recharge locations. These results suggest that aquifer heterogeneity could play an important role in drawdown if a high permeability production zone draws water from an unknown adjacent low permeability zone.

### The Second Calibration

After the initial head distribution and well locations were corrected, the subsidence prediction fair agreement with the U.S.G.S. maps. From Figure 6-3, the major subsidence were occurred between row 5 and row 12 and between column 9 and column 19. The comparisons of subsidence between real data and simulation data are shown in Figures 6-4 to 6-11. From Figures 6-4 and 6-6, the simulation data does not match well with the real data. From Figures 6-5, 6-7, 6-8, 6-9, 6-10, and 6-11, the simulation does reproduce a subsidence in fair agreement with the subsidence in the U.S.G.S. maps. Overall, the simulation model predicts a major subsidence 5 miles south of the real major subsidence. There are two possible reasons for those disagreements in row 5 and row 7. First, in the process of discretization, more than 3,500 pumping wells were digitized and combined into

Figure 6-3 Simulation of Subsidence from 1928-1967

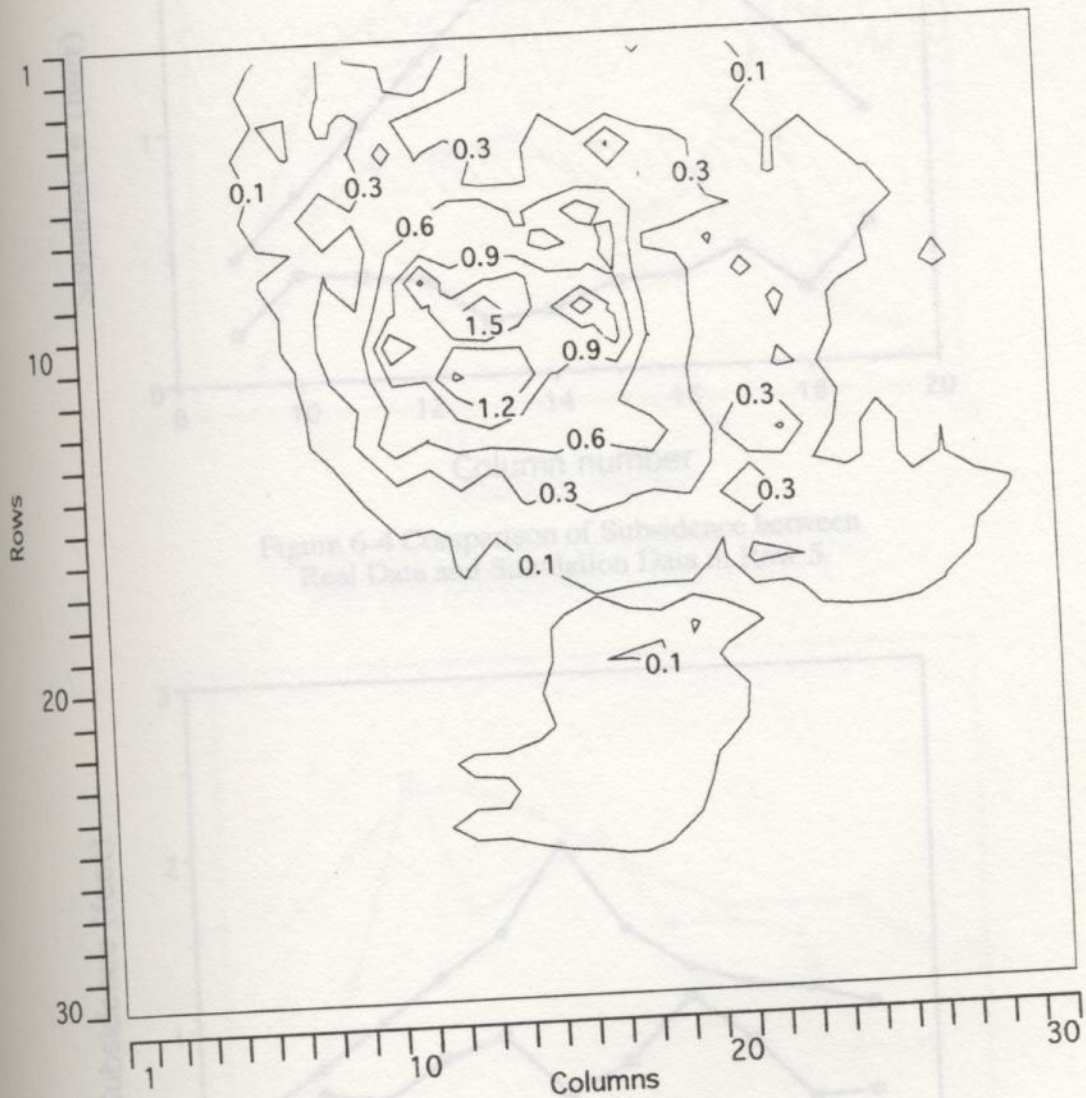


Figure 6-3 Simulation of Subsidence from 1978-1987

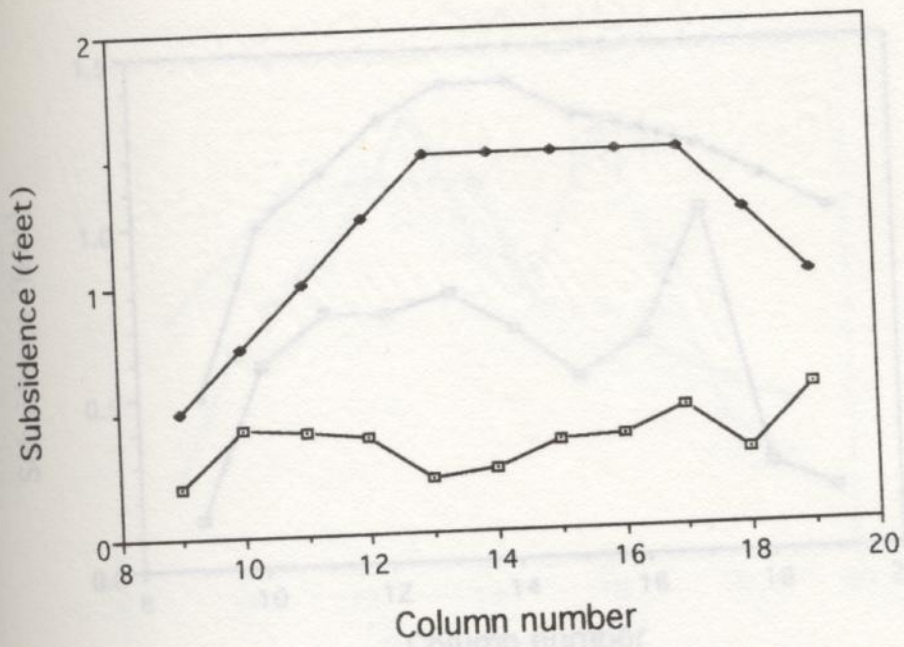


Figure 6-4 Comparison of Subsidence between Real Data and Simulation Data in Row 5

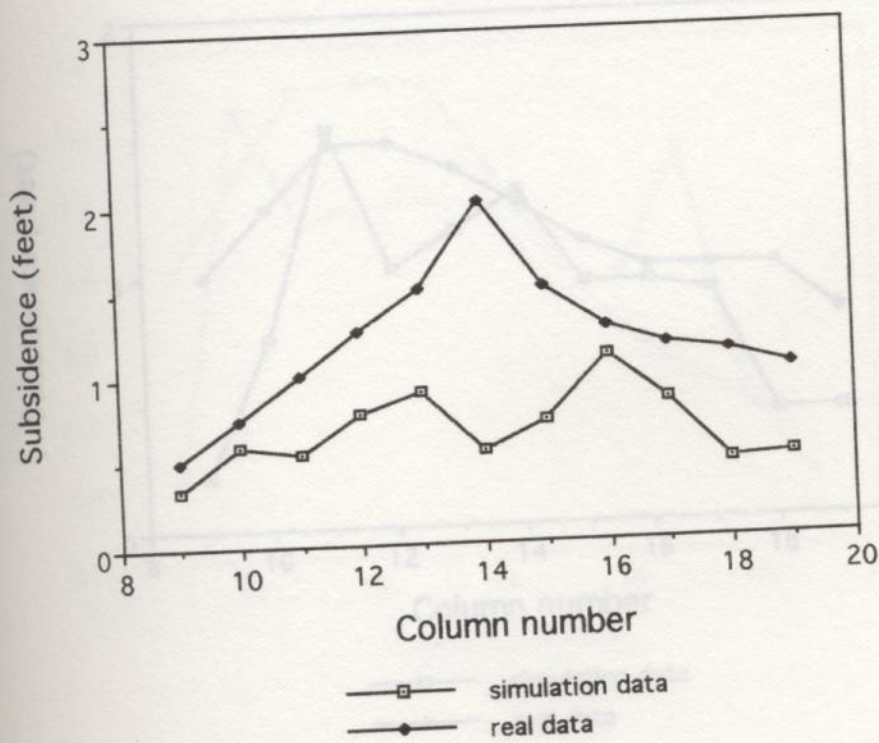


Figure 6-5 Comparison of Subsidence between Real Data and Simulation Data in Row 6

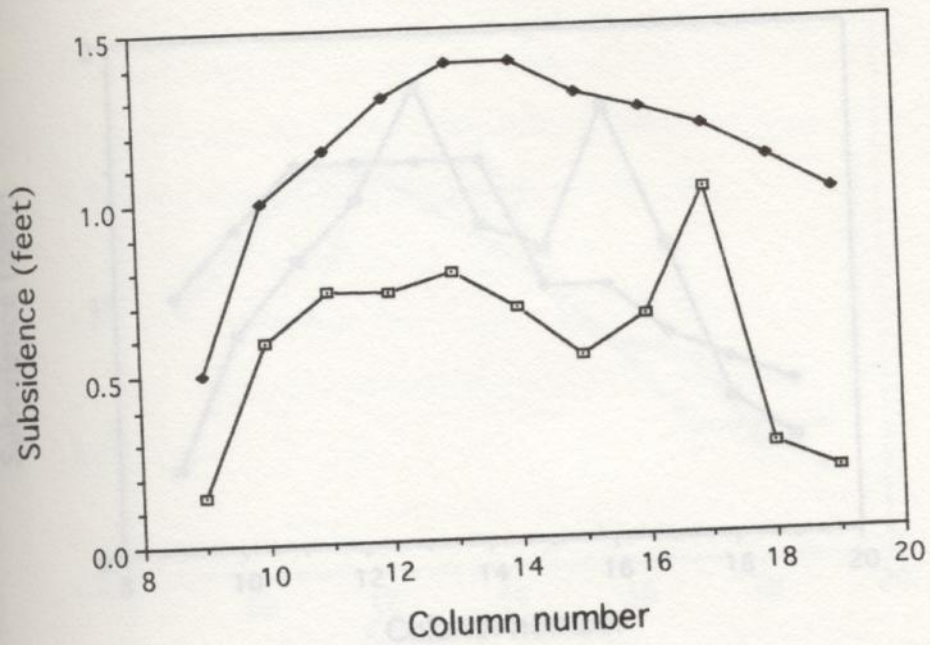


Figure 6-6 Comparison of Subsidence between Real Data and Simulation Data in Row 7

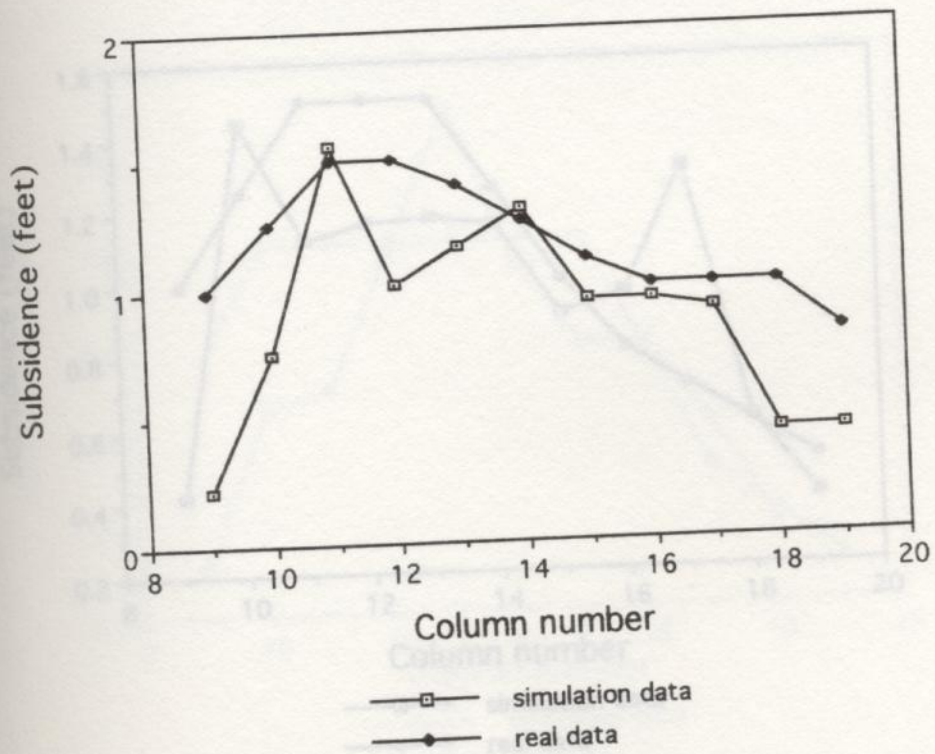


Figure 6-7 Comparison of Subsidence between Real Data and Simulation Data in Row 8



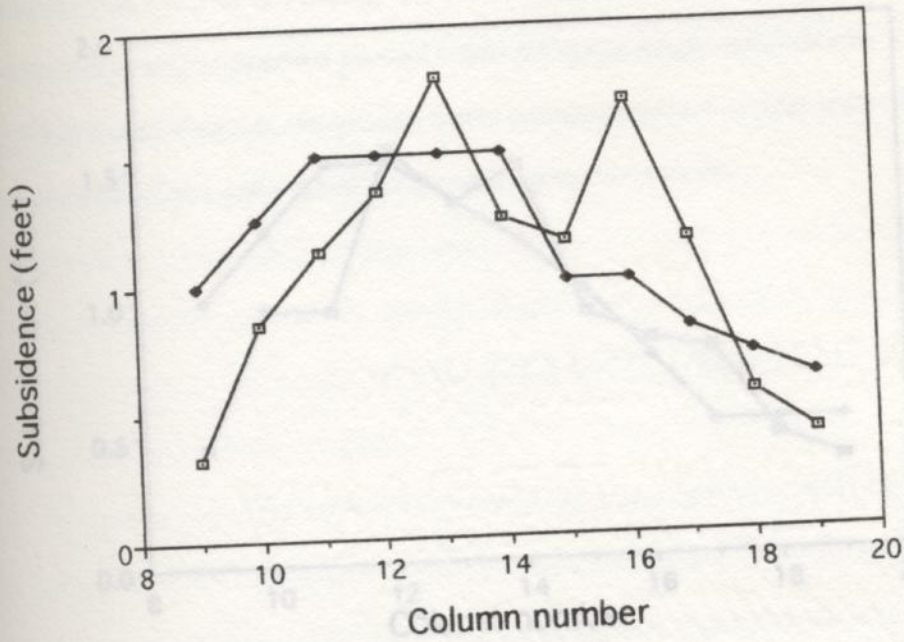


Figure 6-8 Comparison of Subsidence between Real Data and Simulation Data in Row 9

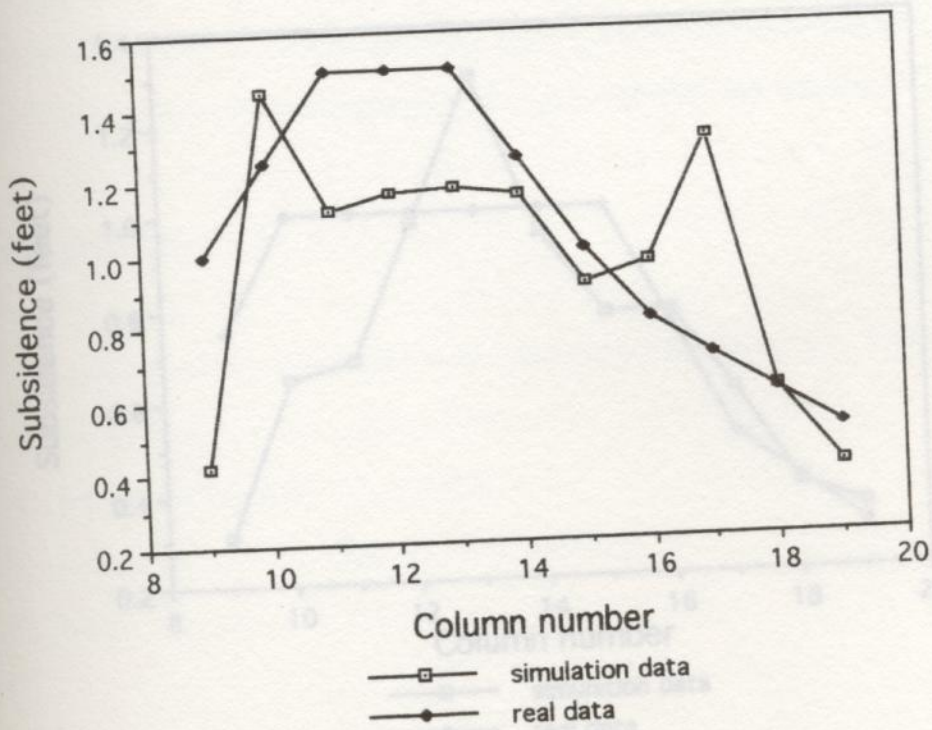


Figure 6-9 Comparison of Subsidence between Real Data and Simulation Data in Row 10

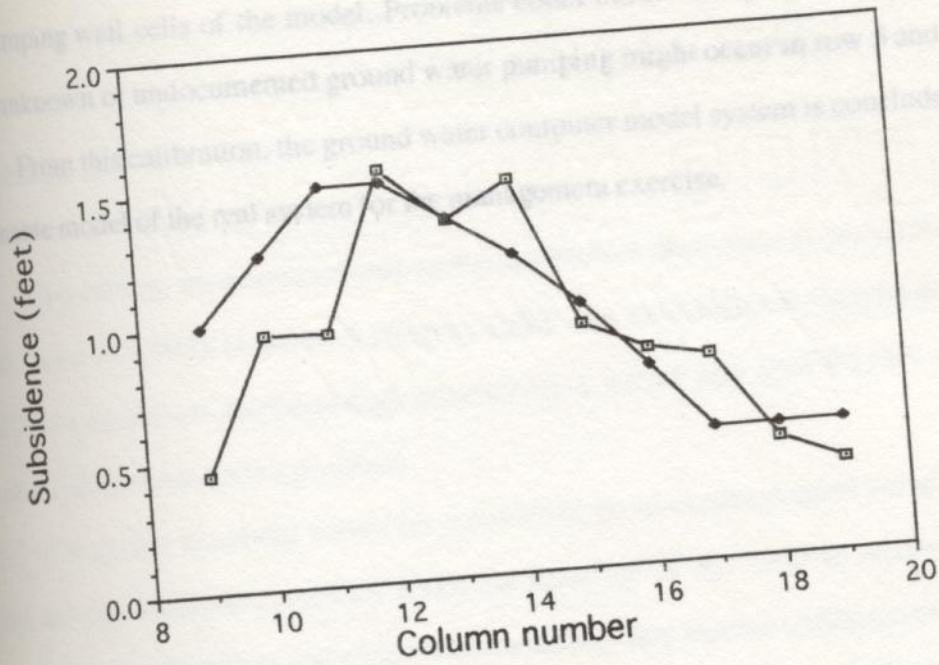


Figure 6-10 Comparison of Subsidence between Real Data and Simulation Data in Row 11

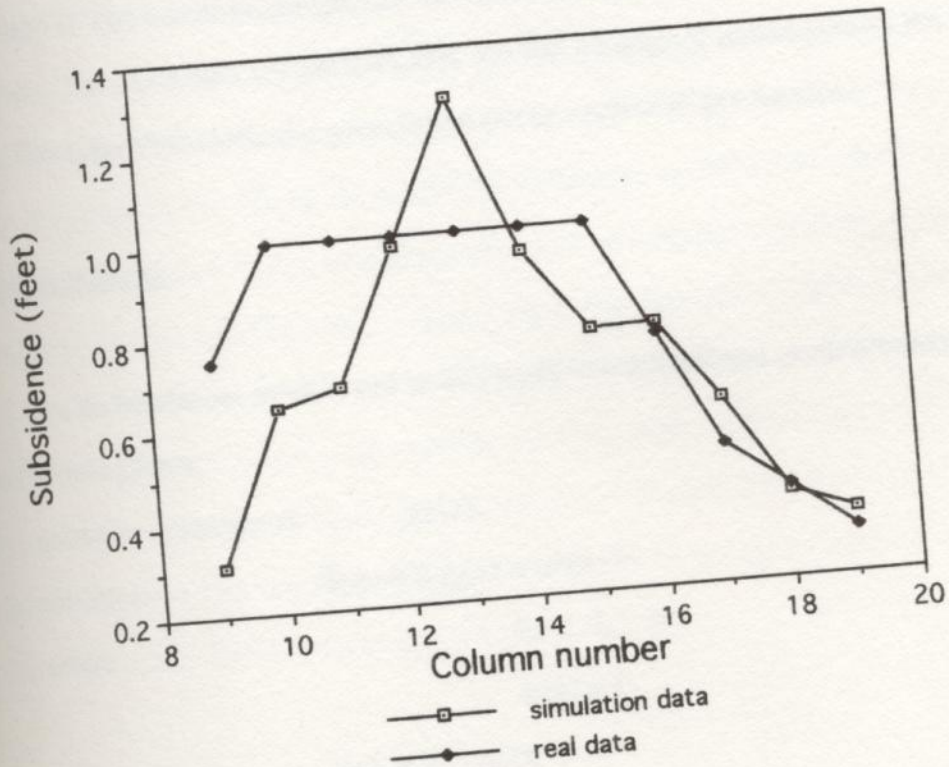


Figure 6-11 Comparison of Subsidence between Real Data and Simulation Data in Row 12

251 pumping well cells of the model. Problems could occur during this process. Second, some unknown or undocumented ground water pumping might occur in row 5 and row 7.

From this calibration, the ground water computer model system is concluded to be a reasonable model of the real system for the management exercise.

The relation method described here is an aquifer management simulator that is a combination of GRG2 (Lasdon & Waren, 1986) and MODFLOW (McDonald, 1988). GRG2 is a nonlinear mathematical programming solver and MODFLOW is a three-dimensional flow simulation program.

The aquifer simulator solves for subsidence given certain control variables. In this study, the subsidence is computed given the pumping of the wells as control variables. This allows the constraints and objective functions of any aquifer optimization problem to be viewed as functions of only these control variables. The input data for GRG2 are the following: (1) The initial pumping; (2) the water demands; and (3) some optimization parameters. The input data for MODFLOW are the geological parameters of the aquifer field. This simulation method is generic and can be applied to any aquifer.

#### Mathematical Model

The mathematical model used in this study was a nonlinear programming problem of the following form:

$$\text{minimize or maximize } z = g(x)$$

$$\text{subject to } h_i(x) \leq g_i(x) \leq ub_i(x),$$

$$\text{where } i = 1, 2, \dots, m,$$

$$\text{and } i \neq k$$

$$lb(x) \leq x_i \leq ub(x)$$

## Chapter 7 Optimization

### Introduction

The solution method described here is an aquifer management simulator that is a combination of GRG2 (Lasdon & Waren, 1989) and MODFLOW (McDonald, 1988). GRG2 is a nonlinear mathematical programming solver and MODFLOW is a three-dimensional flow simulation program.

The aquifer simulator solves for subsidence given certain control variables. In this study, the subsidence is computed given the pumpage of the wells as control variables. This allows the constraints and objective functions of any aquifer optimization problem to be viewed as functions of only these control variables. The input data for GRG2 are the following: (1) The initial pumpage; (2) the water demands; and (3) some optimization parameters. The input data for MODFLOW are the geological parameters of the aquifer model. This simulation method is generic and can be applied to any aquifer.

### Mathematical Model

The mathematical model used in this study was a nonlinear programming problem of the following form:

minimize or maximize  $g_k(x)$ ,

subject to  $lb(n+i) \leq g_i(x) \leq ub(n+i)$ ,

where  $i = 1, 2, \dots, m$ ,

and  $i \neq k$

$$lb(i) \leq x_i \leq ub(i)$$

with  $x$  as a vector of  $n$  real-valued variables,  $g_i$  as real-valued functions of  $x$ ,  $lb$  and  $ub$  as lower bounds and upper bounds, respectively. The objective function  $g_i$  may be linear or nonlinear (Lasdon and Waren, 1989). There are  $m$  such functions, one of which is the objective and the others are equality constraints and inequality constraints.

In this study, the  $x$  vector is the pumping rates of the discharge wells, the objective function is either the minimum subsidence or the minimum energy usage, and the constraints are the ground water demands.

### GRG2

The FORTRAN program GRG2 is used to solve the system of equations; it can solve nonlinear problems by the Generalized Reduced Gradient Method. The user is required to prepare a subroutine GCOMP which computes the values of the objective function and constraints for given variable vector. The user also provides data specifying the upper and lower bounds, as well as other parameters. GRG2 requires an initial solution to start the optimization search. If the initial solution is an infeasible solution, phase I optimization is initiated, which minimizes an objective function consisting of the sum of infeasibilities until a feasible point, is found. Once this feasible solution is achieved, the actual objective function replaces the sum of infeasibilities and the actual optimization phase is initiated. Using an initial point provided by the user, allows the inclusion of engineering judgment in selecting a good initial solution. Although the model is able to give an optimal solution to the problem, the optimal solution may not be the global optimal solution. A simple flowchart of GRG2 is presented in Figure 7-1.

Figure 7-1 Flowchart of GRG2 (modified from Lansey & Mays 1989)

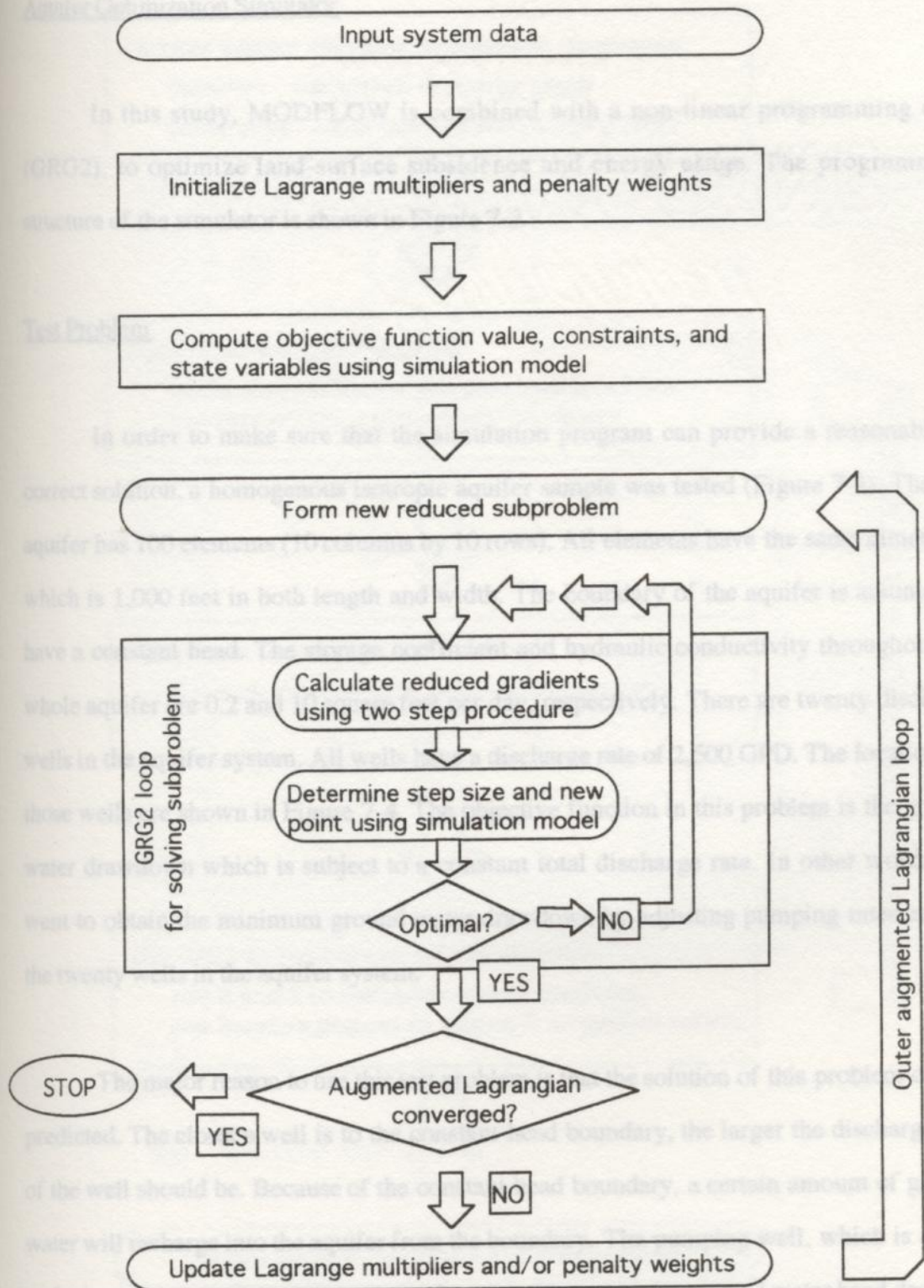


Figure 7-1 Flowchart of GRG2 (modified from Lansey & Mays 1989)

### Aquifer Optimization Simulator

In this study, MODFLOW is combined with a non-linear programming code (GRG2), to optimize land-surface subsidence and energy usage. The programming structure of the simulator is shown in Figure 7-2.

### Test Problem

In order to make sure that the simulation program can provide a reasonable or correct solution, a homogenous isotropic aquifer sample was tested (Figure 7-3). The test aquifer has 100 elements (10 columns by 10 rows). All elements have the same dimension which is 1,000 feet in both length and width. The boundary of the aquifer is assumed to have a constant head. The storage coefficient and hydraulic conductivity throughout the whole aquifer are 0.2 and 10 square feet per day, respectively. There are twenty discharge wells in the aquifer system. All wells have a discharge rate of 2,500 GPD. The locations of those wells are shown in Figure 7-4. The objective function in this problem is the ground water drawdown which is subject to a constant total discharge rate. In other words, we want to obtain the minimum ground water drawdown by adjusting pumping rates among the twenty wells in the aquifer system.

The major reason to use this test problem is that the solution of this problem can be predicted. The closer a well is to the constant-head boundary, the larger the discharge rate of the well should be. Because of the constant head boundary, a certain amount of ground water will recharge into the aquifer from the boundary. The pumping well, which is closer to the boundary, can pump more ground water without causing ground water head decline.

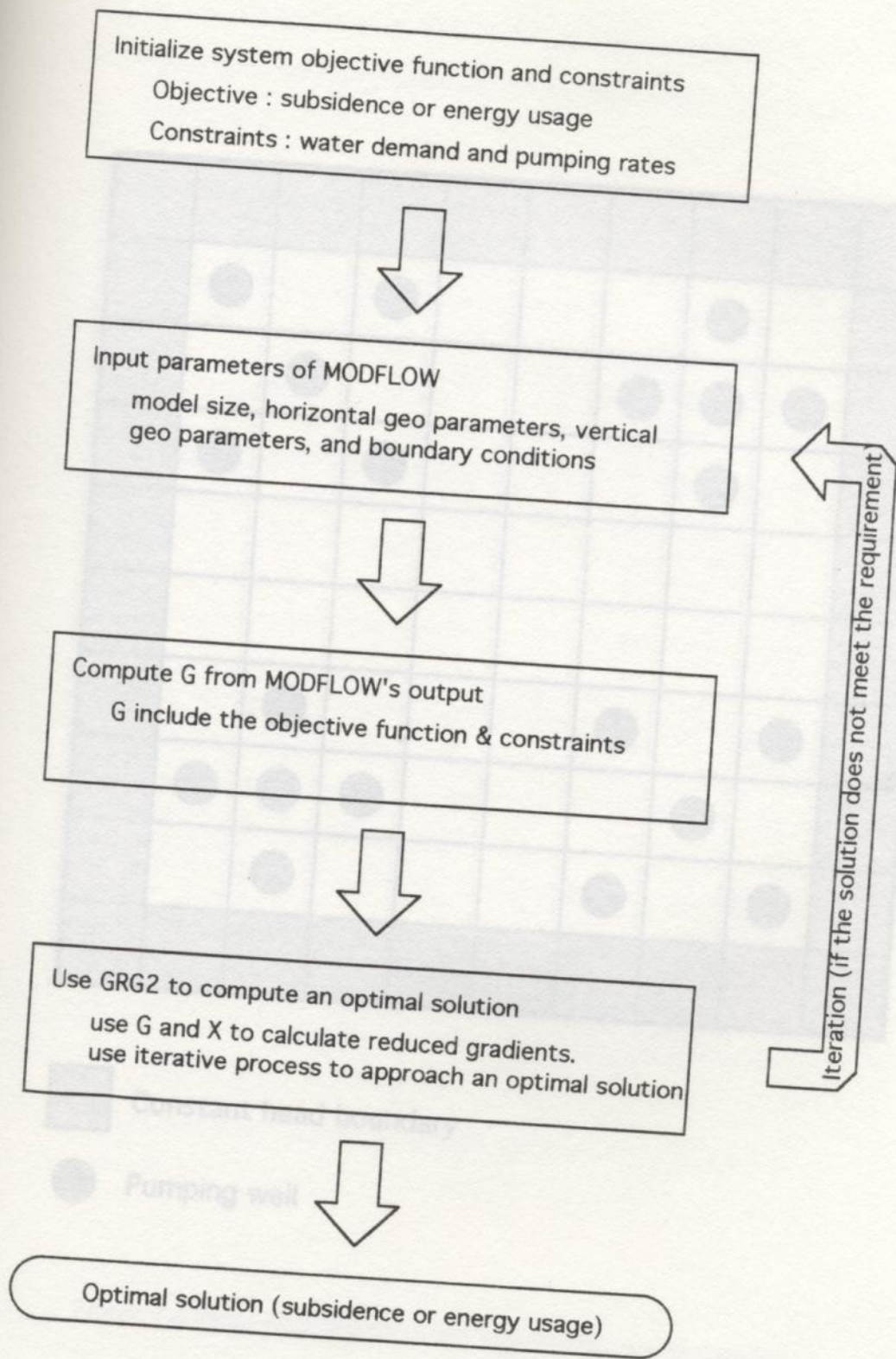
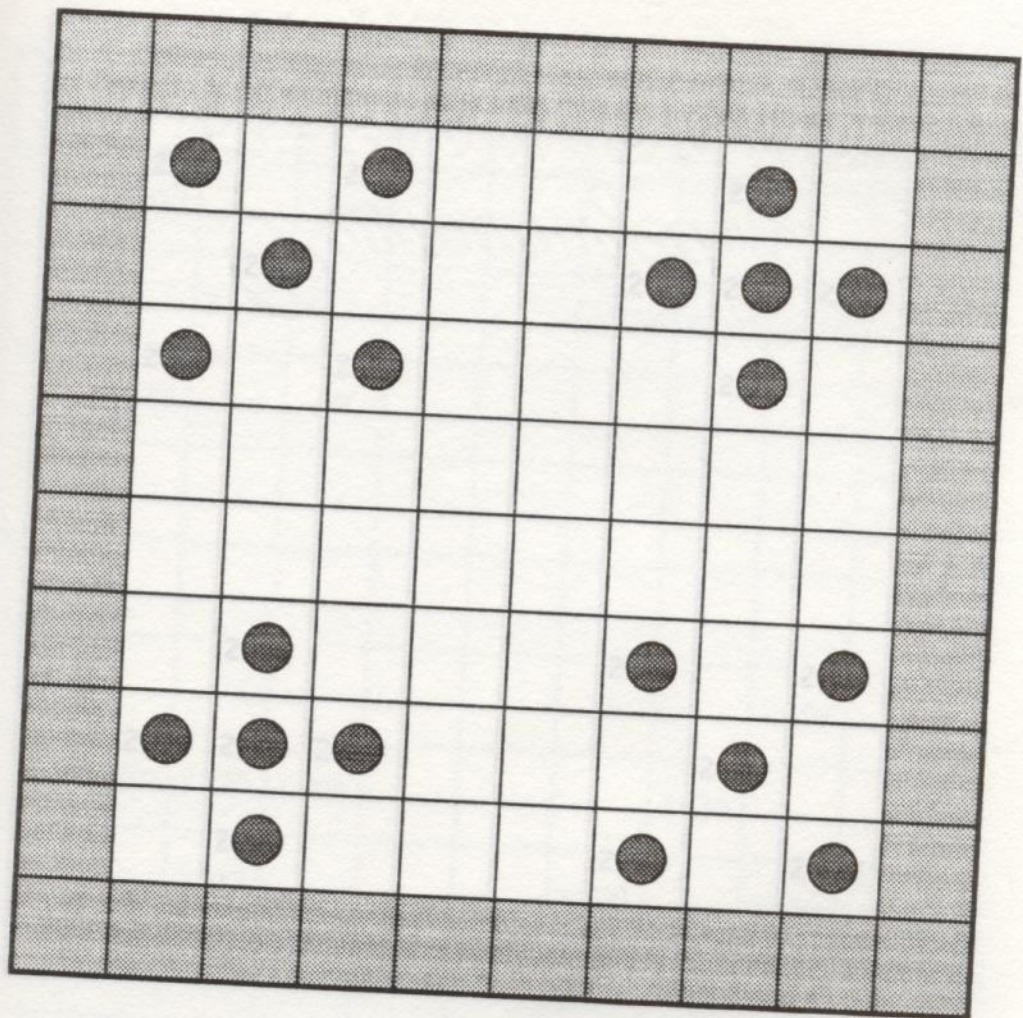


Figure 7-2 Flowchart of the Optimal Simulator





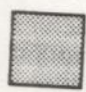

-  Constant head boundary
-  Pumping well

Figure 7-4 Pump Distribution of the Aquifer before Optimization

Figure 7-3 The One-layer Homogenous Aquifer Test Problem

The simulator provides a result that agreed with the predicted result shown in Figure 7-5. Therefore it is concluded that the optimization approach is reasonable.

	2500		2500				2500		
		2500				2500	2500	2500	
	2500		2500				2500		
		2500				2500		2500	
	2500	2500	2500				2500		
		2500				2500		2500	

Figure 7-5 Pump Distribution of the Aquifer after Optimization

Figure 7-4 Pump Distribution of the Aquifer before Optimization

The simulator provides a result that agreed with the predicted trend (shown in Figure 7-5). Therefore it is concluded that the optimization approach is reasonable.

Ground Water Simulation

	3500		3500				3500	
		2765				1935	2220	3470
	3422		49				767	
		0				0		3256
	3500	2300	2150				2826	
		3343				3500		3500

Figure 7-5 Pump Distribution of the Aquifer after Optimization

The simulation-optimization model was run on a Next PS computer for 48 hours. The result of optimal subsidence simulation provides a 55% reduction of total subsidence function without decreasing the ground water discharge rate. The optimized simulation

## Chapter 8 Optimal Subsidence Simulation

### Ground Water Simulation

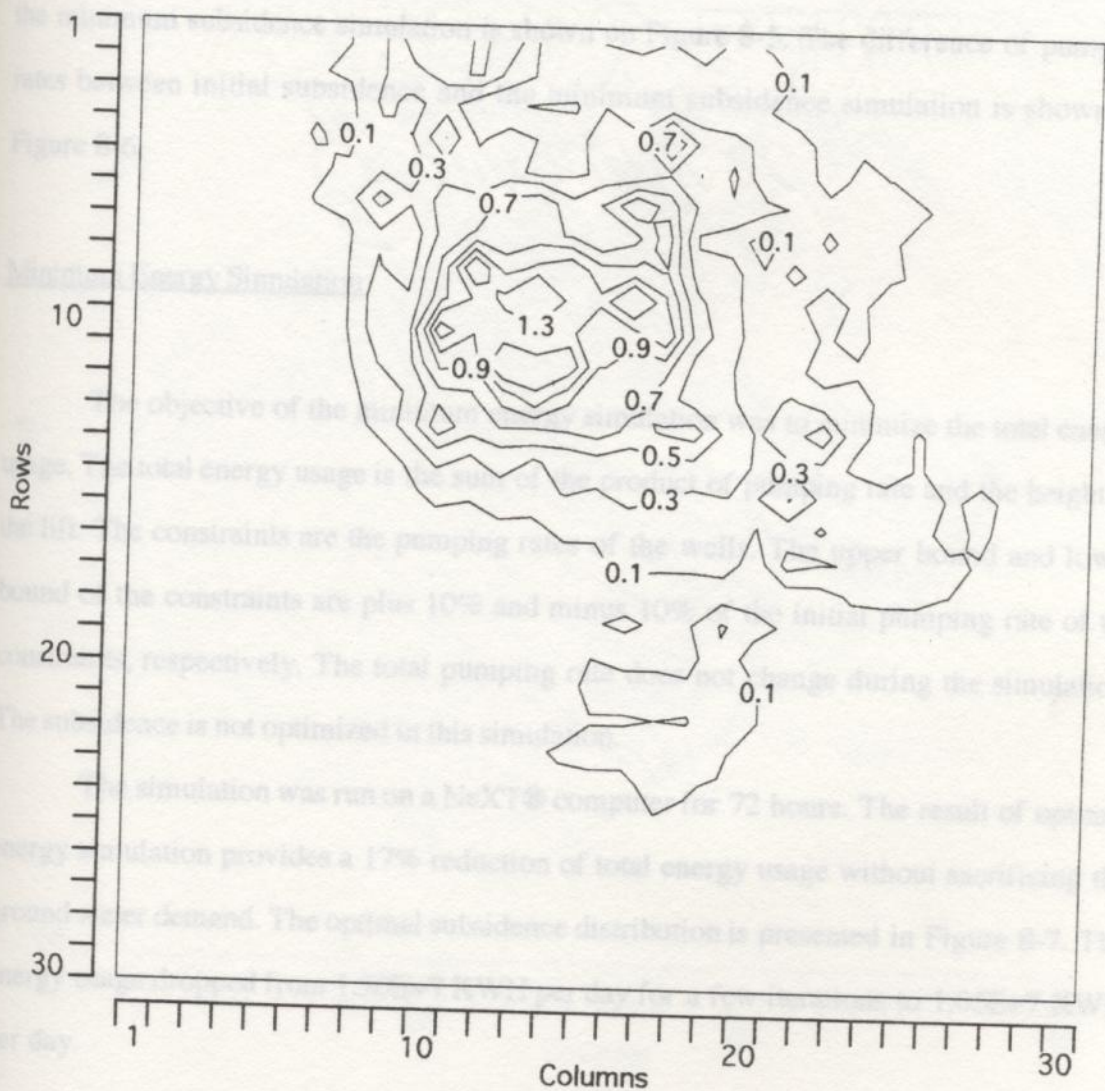
There are more than 3,000 pumping wells in the model area. The initial pumping rates used in this study are the average rates during the period between 1978 and 1987. The pumping rates of the wells vary from 90 gallons per day to 18,700,000 gallons per day. In this study, those wells are digitized and located into 251 cells of the aquifer system. The constraints of the study are the pumping rate of the wells. Using digitization, the constraints' number was reduced from more than 3,000 to 251. However, 251 constraints are still too many for the optimization program. The wells with pumping rate less than 1 MGD were set as constant pumping wells. The number of constraints is now further reduced to 100. The subsidence contour distribution before optimization is presented in Figure 8-1.

### Minimum Subsidence Simulation

The objective of the minimum subsidence simulation was to minimize the total subsidence. The objective function is the sum of the squared subsidence of each element. The constraints are the pumping rates of the wells. The upper bound and lower bound of the constraints are plus 10% and minus 10% of the initial pumping rate of the constraints, respectively. The total pumping rate does not change during the simulation. The energy usage is not optimized in this simulation.

The simulation-optimization model was run on a NeXT® computer for 48 hours. The result of optimal subsidence simulation provides a 5% reduction of total subsidence function without decreasing the ground water discharge rate. The optimized simulation

subidence contour is shown in Figure 8-2. The sum of square subidence drops from about 80 square feet for a few iterations to around 70.5 square feet. Three-dimensional surface plots for both the initial subidence and the minimum subidence simulation are shown in Figures 8-3 and 8-4. The difference of subidence between initial subidence and



**Comparison**

From Figures 8-1, 8-2, 8-3, 8-4, 8-5, and 8-6, it is obvious that the major subsidence occurs in the **Figure 8-1 Initial Subsidence Distribution** aquifer model.

subsidence contour is shown in Figure 8-2. The sum of square subsidence drops from about 80 square feet for a few iterations to around 70.5 square feet. three-dimensional surface plots for both the initial subsidence and the minimum subsidence simulation are shown in Figures 8-3 and 8-4. The difference of subsidence between initial subsidence and the minimum subsidence simulation is shown on Figure 8-5. The difference of pumping rates between initial subsidence and the minimum subsidence simulation is shown on Figure 8-6.

#### Minimum Energy Simulation

The objective of the minimum energy simulation was to minimize the total energy usage. The total energy usage is the sum of the product of pumping rate and the height of the lift. The constraints are the pumping rates of the wells. The upper bound and lower bound of the constraints are plus 10% and minus 10% of the initial pumping rate of the constraints, respectively. The total pumping rate does not change during the simulation. The subsidence is not optimized in this simulation.

The simulation was run on a NeXT® computer for 72 hours. The result of optimal energy simulation provides a 17% reduction of total energy usage without sacrificing the ground water demand. The optimal subsidence distribution is presented in Figure 8-7. The energy usage dropped from  $1.30E+7$  KWH per day for a few iterations to  $1.05E+7$  KWH per day.

#### Comparisons

From Figures 8-1, 8-2, 8-3, 8-4, 8-5, and 8-6, it is obvious that the major subsidence occurs in the area of the rows 8, 9, 10, 11, and 12 of the aquifer model.

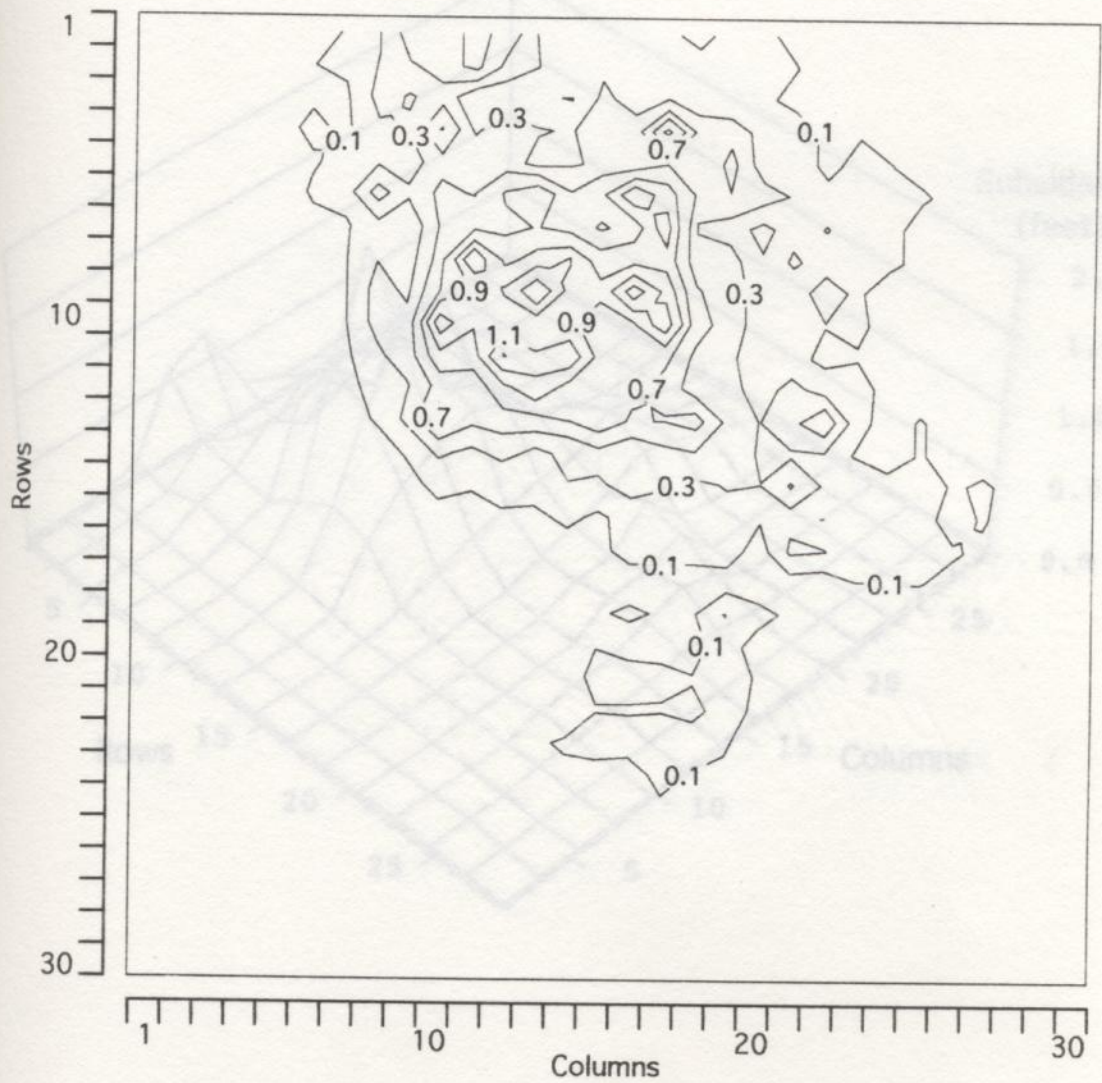


Figure 8-2 Simulated Subsidence Distribution (Minimum Subsidence)

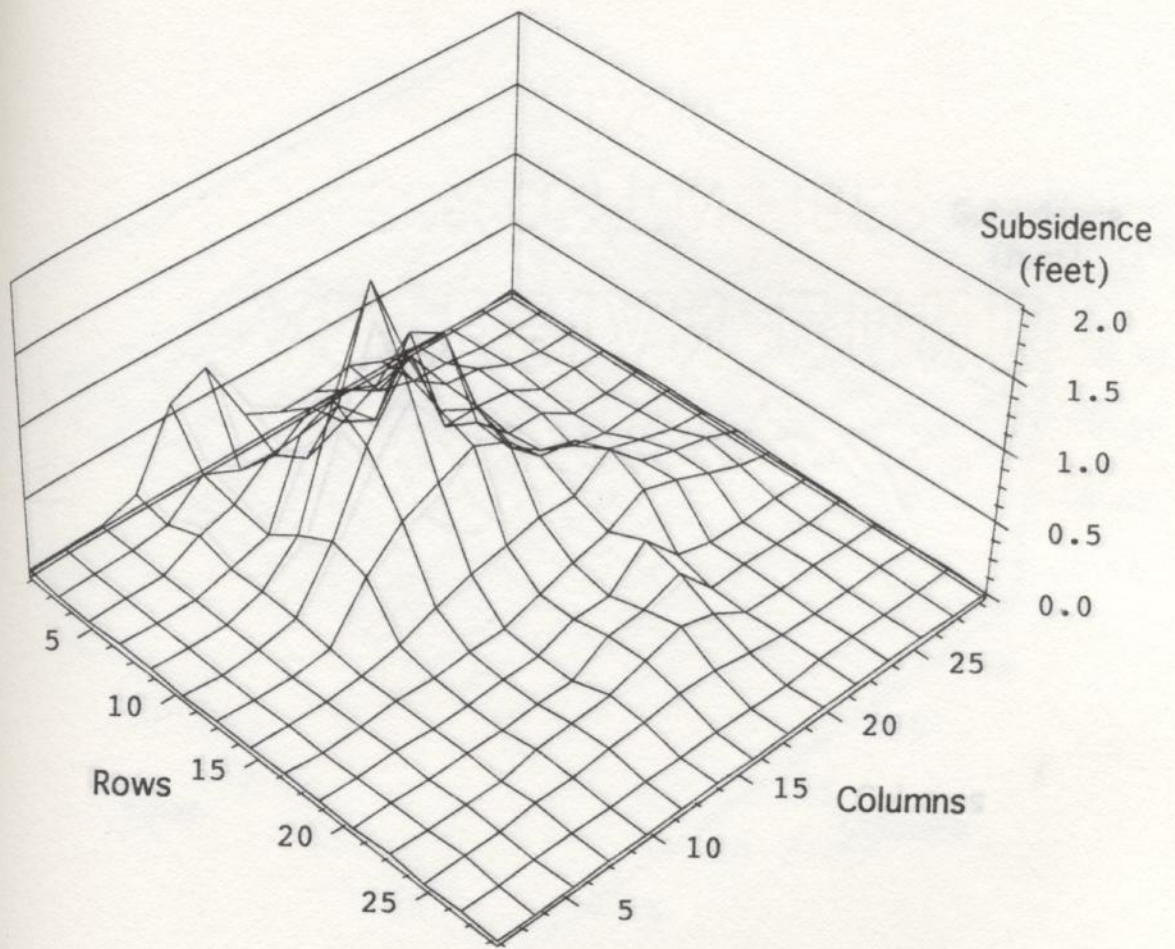


Figure 8-3 Surface Plot of Initial Subsidence



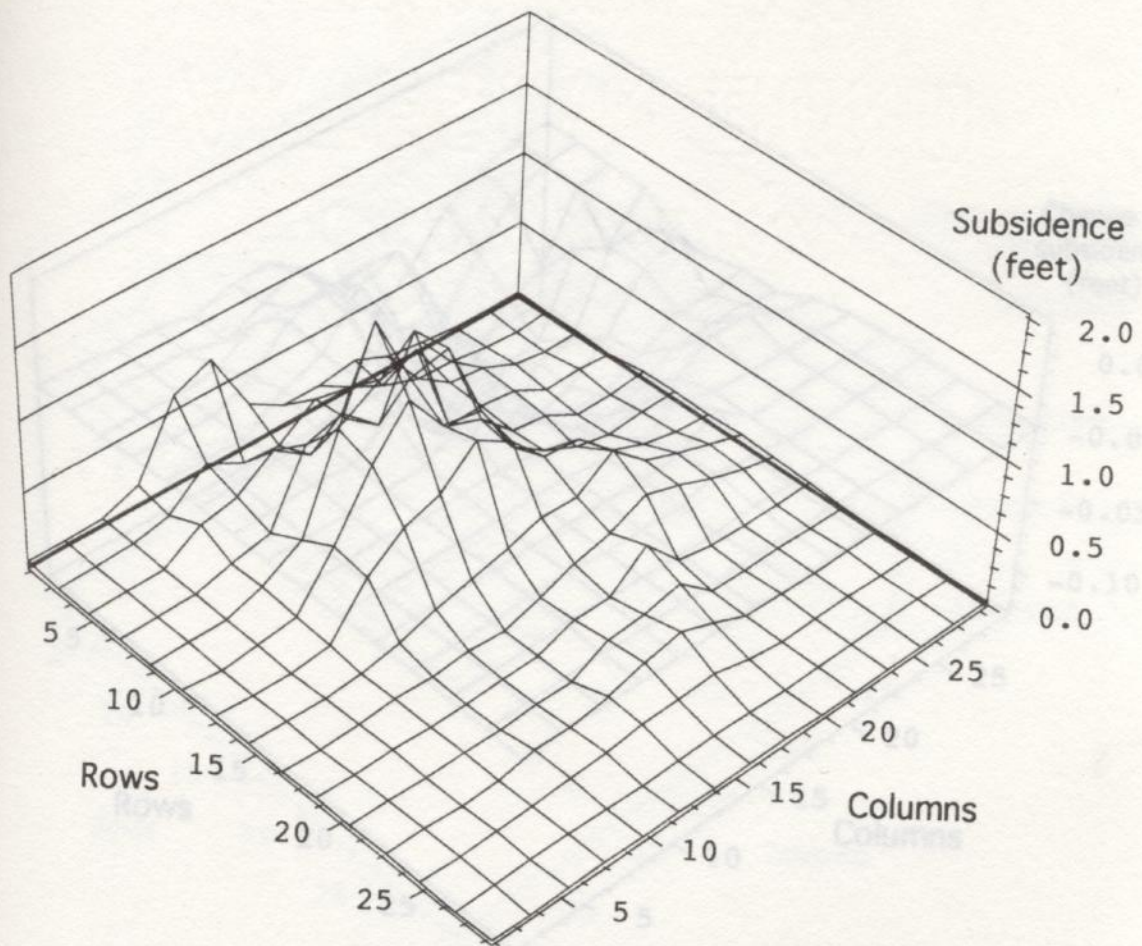


Figure 8-3 Surface Plot of The Difference between Initial Subsidence

Figure 8-4 Surface Plot of Minimum Subsidence Simulation

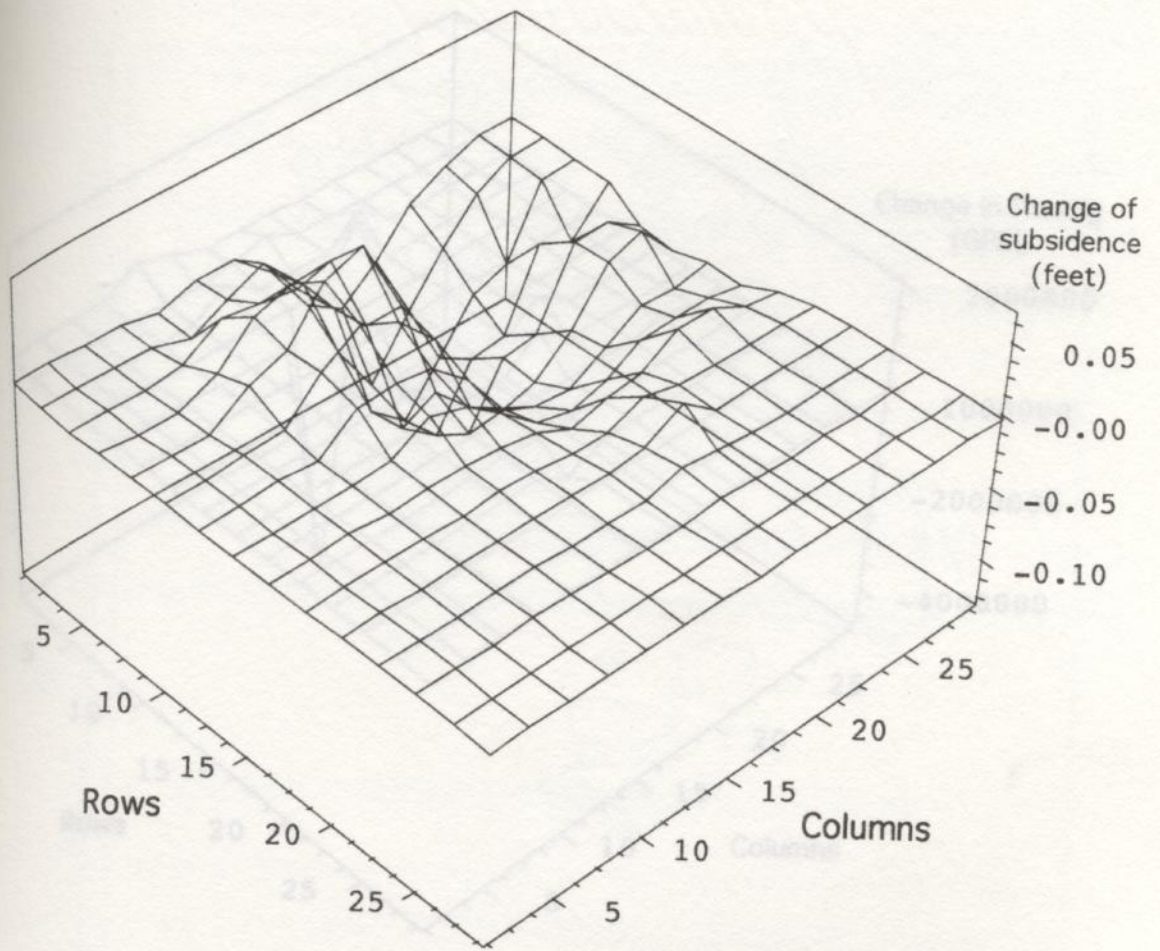


Figure 8-5 Surface Plot of The Difference between Initial Subsidence and Minimum Subsidence Simulation

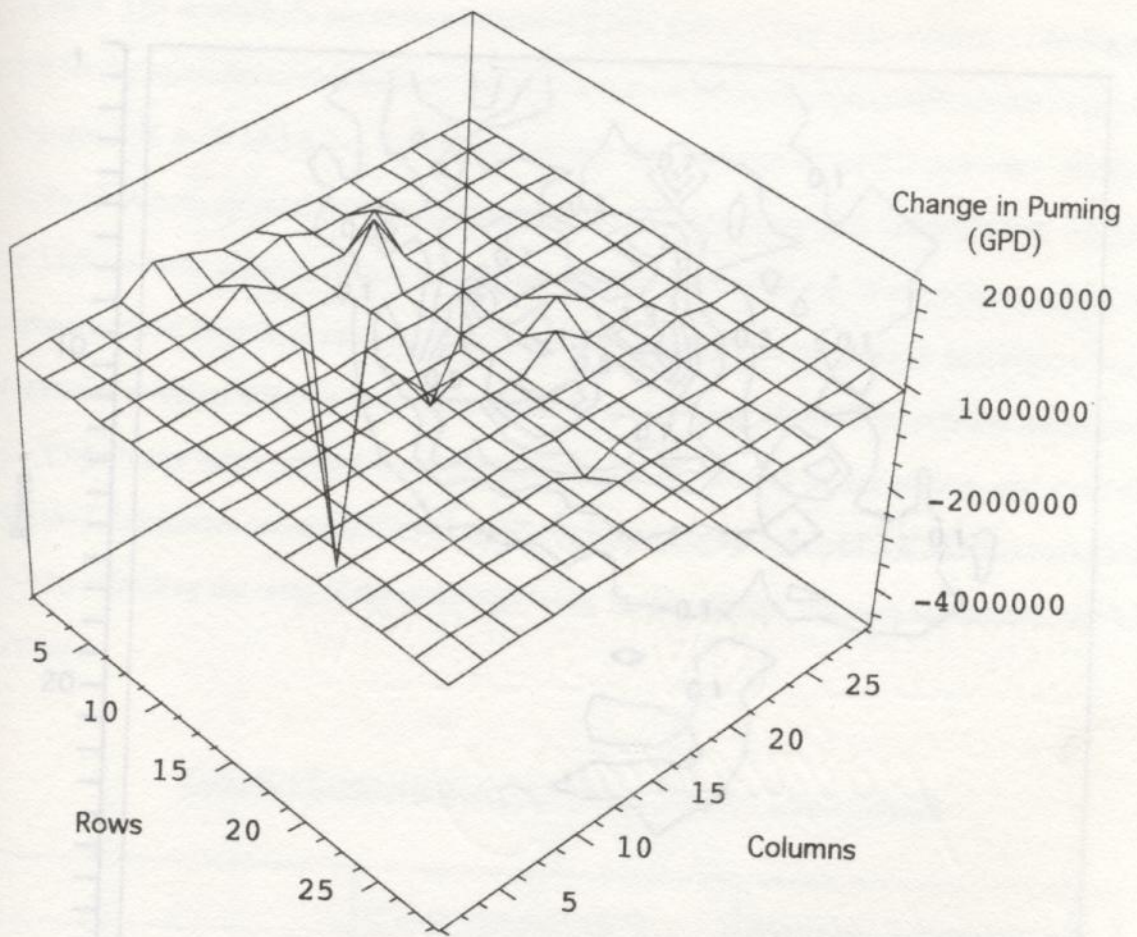


Figure 8-6 Change of Pumping Rate between Initial Subsidence and Minimum Subsidence Simulation

Figures 8-8 to 8-12 show the comparisons of subsidence between the original model, the minimum subsidence model, and the minimum energy usage model for rows 8, 9, 10, 11 and 12, respectively. From Figures 8-8 to 8-12, the subsidence are reduced in both optimal models. The subsidence are reduced about 0.3 foot and 0.2 foot near criteria 12 in Figure 8-8 (minimum subsidence model) and 0.2 foot near criteria 12 in Figure 8-9 (minimum energy usage model), respectively. In Figures 8-10 and 8-11, the subsidence are reduced about 0.2 foot near criteria 12 and 0.1 foot near criteria 10 to 11, respectively. In Figure 8-12, the subsidence are reduced about 0.1 foot near criteria 12 and 0.1 foot near criteria 10 to 11, respectively. The subsidence are reduced about 0.1 foot near criteria 12 and 0.1 foot near criteria 10 to 11, respectively. The subsidence are reduced about 0.1 foot near criteria 12 and 0.1 foot near criteria 10 to 11, respectively.

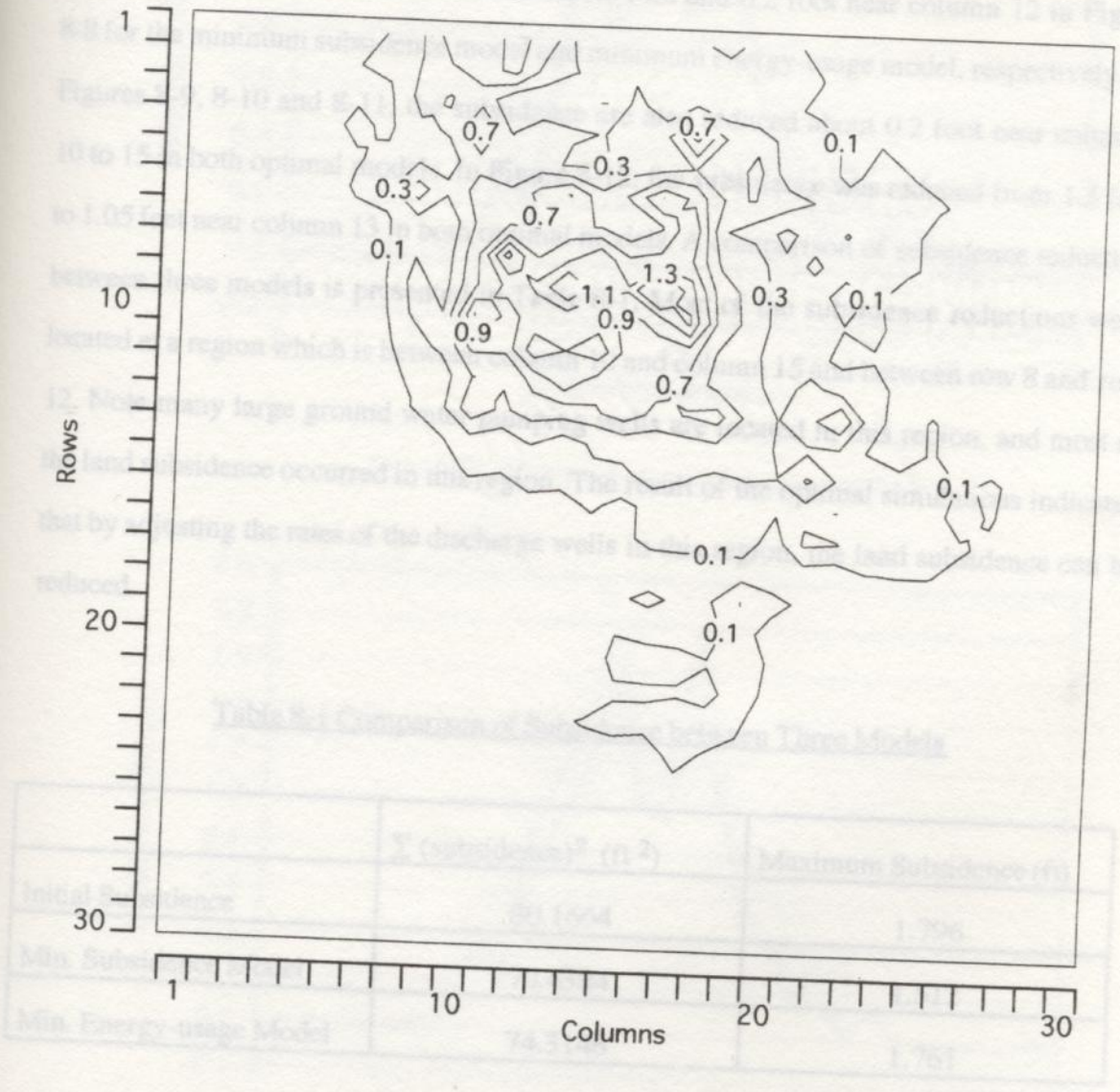


Figure 8-7 Simulated Subsidence Distribution (Minimum Energy)

Figures 8-8 to 8-12 show the comparisons of subsidence between the original model, the minimum subsidence model, and the minimum energy-usage model for rows 8, 9, 10, 11, and 12, respectively. From Figures 8-8 to 8-12, the subsidence are reduced in both optimal models. The subsidence are reduced about 0.3 foot and 0.2 foot near column 12 in Figure 8-8 for the minimum subsidence model and minimum energy-usage model, respectively. In Figures 8-9, 8-10 and 8-11, the subsidence are also reduced about 0.2 foot near columns 10 to 15 in both optimal models. In Figure 8-12, the subsidence was reduced from 1.3 feet to 1.05 feet near column 13 in both optimal models. A comparison of subsidence reduction between three models is presented in Table 8-1. Most of the subsidence reductions were located at a region which is between column 10 and column 15 and between row 8 and row 12. Note many large ground water pumping wells are located in this region, and most of the land subsidence occurred in this region. The result of the optimal simulations indicated that by adjusting the rates of the discharge wells in this region, the land subsidence can be reduced.

Table 8-1 Comparison of Subsidence between Three Models

	$\Sigma (\text{subsidence})^2 (\text{ft}^2)$	Maximum Subsidence (ft)
Initial Subsidence	80.1664	1.796
Min. Subsidence Model	70.4384	1.512
Min. Energy-usage Model	74.3148	1.761

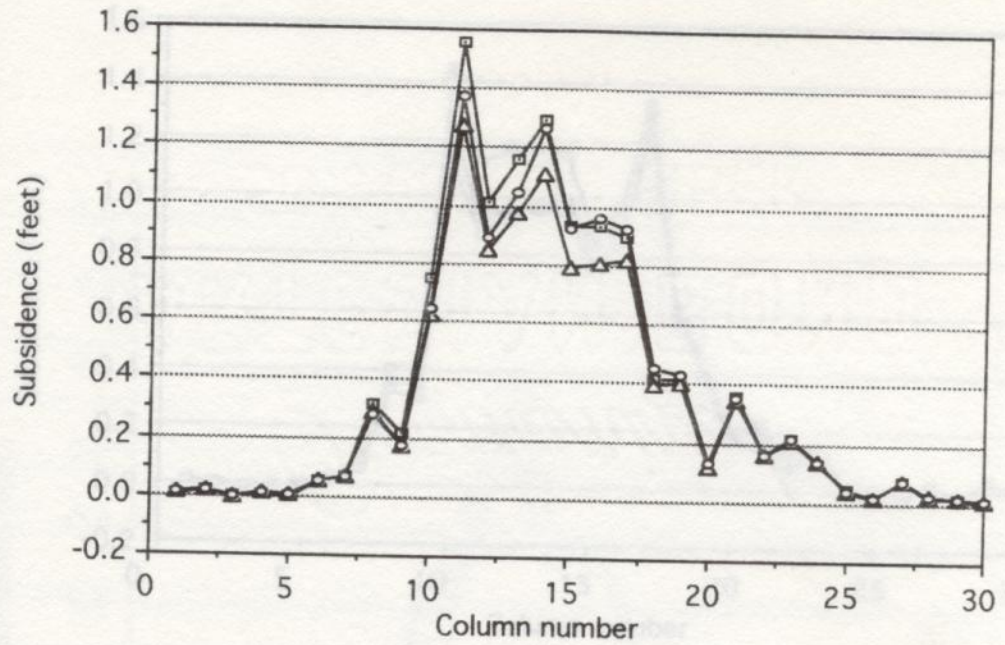


Figure 8-8 Comparison of subsidence in Row 8

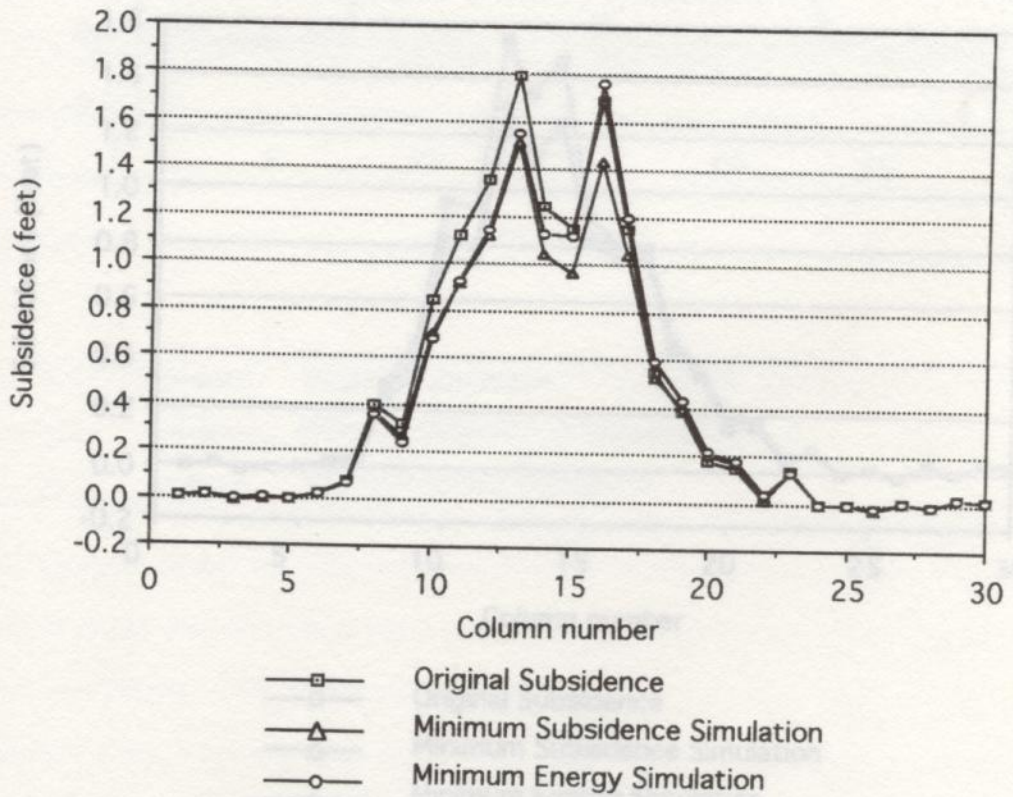


Figure 8-9 Comparison of Subsidence in Row 9

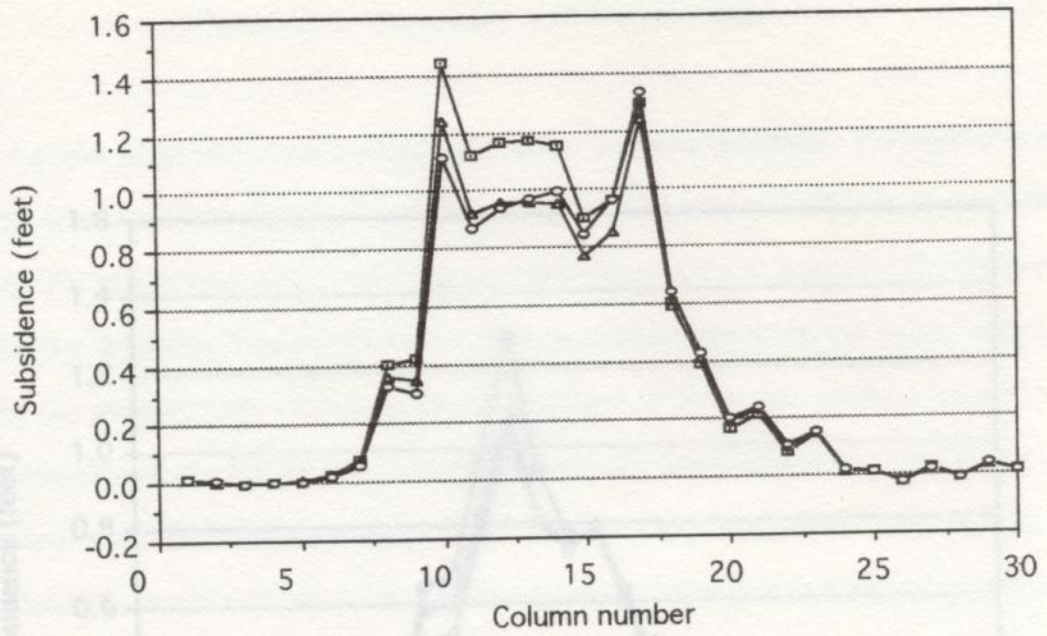


Figure 8-10 Comparison of Subsidence in Row 10

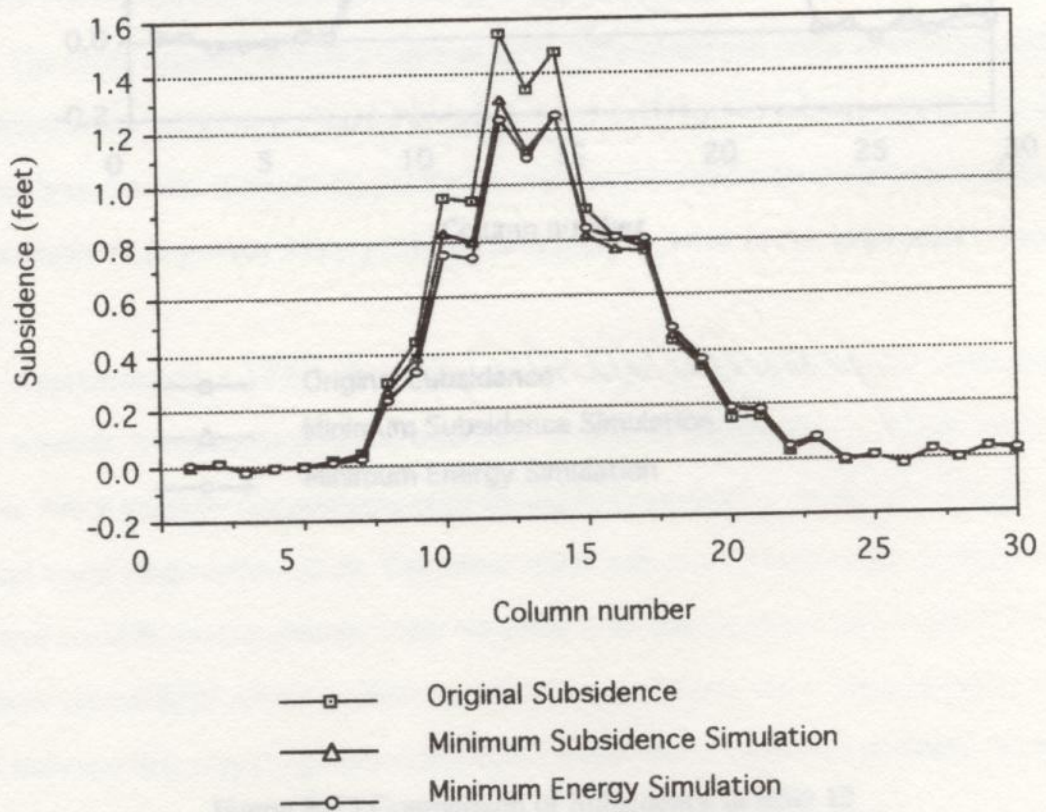
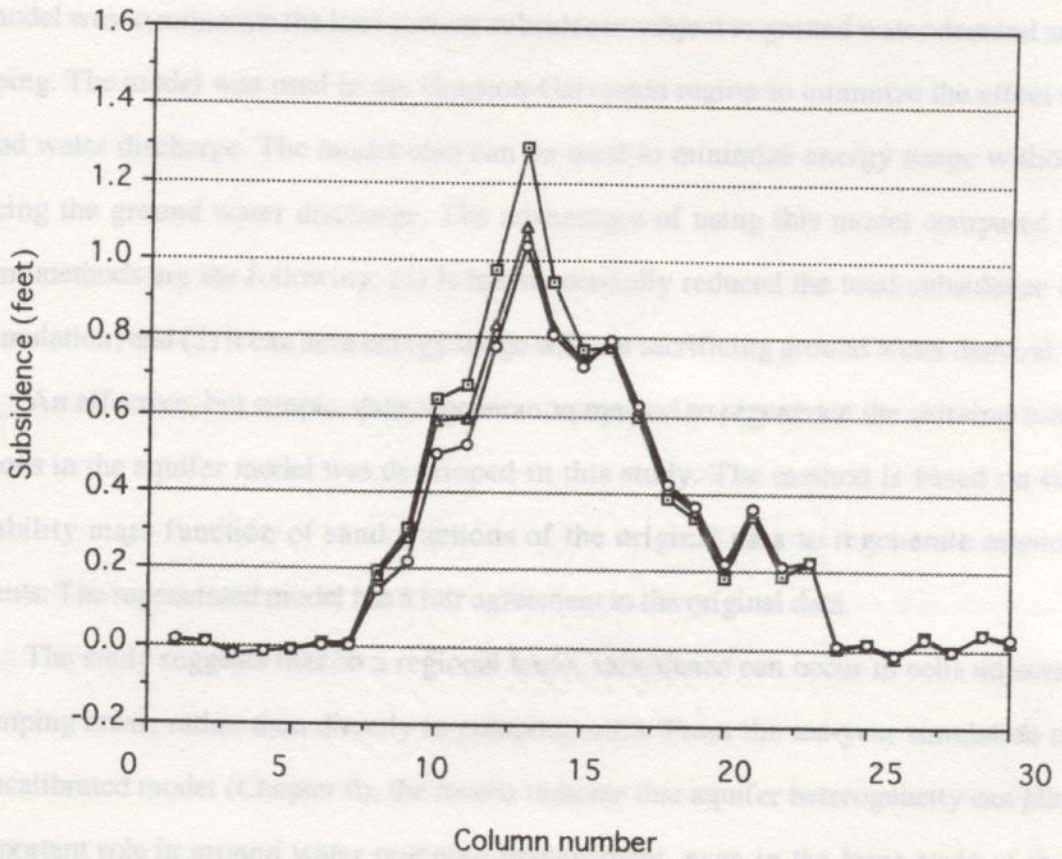


Figure 8-11 Comparison of Subsidence in Row 11



- Original Subsidence
- △— Minimum Subsidence Simulation
- Minimum Energy Simulation

Figure 8-12 Comparison of Subsidence in Row 12



## Chapter 9 Summary and Conclusions

An optimal ground water management model has been presented. The objective of the model was to minimize the land surface subsidence subject to ground water demand and pumping. The model was used in the Houston-Galveston region to minimize the effect of ground water discharge. The model also can be used to minimize energy usage without reducing the ground water discharge. The advantages of using this model compared to current methods are the following: (1) It has successfully reduced the total subsidence in the simulation; and (2) it can save energy usage without sacrificing ground water demand.

An effective, but simple, data regeneration method to regenerate the missing sand fractions in the aquifer model was developed in this study. The method is based on the probability mass function of sand fractions of the original data to regenerate missing elements. The regenerated model has a fair agreement to the original data.

The study suggests that on a regional basis, subsidence can occur in cells adjacent to pumping areas, rather than directly in pumping areas. From the ten-year simulation of the uncalibrated model (Chapter 6), the results indicate that aquifer heterogeneity can play an important role in ground water pumping management, even in the large scale of this model.

Approximately a 17% reduction in energy usage can be achieved for a minimal energy solution. A minimum subsidence solution uses more energy than a minimal energy solution, which suggests that pumping costs should be considered as an important factor of a ground water usage optimization. This observation indicates that economic management incentives could be used to manage water resources (i.e., make it less costly to pump from deep over-consolidated units by assessing subsidence penalties, etc.). Unfortunately, the model indicates that extracting reasonably useful quantities of water will probably always cause some subsidence, although this scenario was not thoroughly explored.

The maximum subsidence of the minimum energy solution is close to the initial condition. This result indicates that a carefully designed optimal pumping strategy may not reduce land-surface subsidence in certain areas, but it can save energy. If surface water rights become scarce, or surface water quality is compromised, economic management of ground water will become a very important issue. The balance between minimal subsidence requirements and economic use of energy is a practical problem beyond the scope of this study.

There are three limitations of the model. First, the resulting pumpage rate of wells may not be achievable at local pump stations due to equipment used at the stations. The second is that the model requires considerable computational effort to determine the optimal ground water pumping rates of a ground water aquifer model with many pumping wells. Third, the pumping efficiency and hydraulic conditions are not considered in the current version of the model. Since those two conditions were not included in this study, the saving of the energy may not reflect real world conditions. However, the upper bound and lower bound of the constraints were set at plus 10% and minus 10% of the initial pumping rate of the constraints, respectively. This step should prevent unrealistic solutions. These limitations should be tested in future research.

Gabrysch, R.N. (1964). "Ground Water Withdrawals and Land-surface Subsidence in the Houston-Galveston Region, Texas, 1946-60." U.S. Geological Survey Report 267.

Gabrysch, R.N., and Bunnell, C.W. (1973). "Land-surface Subsidence in the Houston-Galveston Region, Texas." Texas Water Development Board, Report 138, p. 19.

Gabrysch, R.N., and Coplin, L.S. (1980). "Land-surface Subsidence Resulting from Ground-water Withdrawals in the Houston-Galveston Region, Texas, through 1987." Report of Investigations No. 80-01. Prepared by U.S. Geological Survey in cooperation with the Harris-Galveston Coastal Subsidence District.

## References

- Bravo, R. (1990). "Prediction of Houston Ground-Water Heads and Land Subsidence using Three-Dimensional Finite Differences." Ph.D. Dissertation, Department of Civil and Environmental Engineering, University of Houston.
- Callaway, R. (1985). "Harris-Galveston Coastal Subsidence District - A Report on its Creation, Powers, Limitations of Powers, and Progress." *Issues in Ground Water Management*, Center for Research in Water Resources, Austin, TX.
- Casola, W.H., Narayanan, R., Duffy, C., and Bishop, A.B. (1986). "Optimal Control Model for Ground Water Management." *Journal of Water Resources Planning and Management*, American Society of Civil Engineers, 112(2), 183-197.
- Duan, N., Mays, L.W., and Lansey, K.E. (1990). "Optimal Reliability-based Design of Pumping and Distribution Systems." *Journal of Hydraulic Engineering*, American Society of Civil Engineers, 116(2), 249-269.
- Gabrysch, R.K. (1984). "Ground Water Withdrawals and Land-surface Subsidence in the Houston-Galveston Region, Texas, 1906-80." *U. S. Geological Survey Report 287*.
- Gabrysch, R.K., and Bonnet, C.W. (1975). "Land-surface Subsidence in the Houston-Galveston Region, Texas." *Texas Water Development Board*, Report 188, p.19.
- Gabrysch, R.K., and Coplin, L.S. (1990). "Land-surface Subsidence Resulting from Ground-water Withdrawals in the Houston-Galveston Region, Texas, through 1987." *Report of Investigations No. 90-01*, Prepared by U.S. Geological Survey in cooperation with the Harris-Galveston Coastal Subsidence District.

- Harris-Galveston Coastal Subsidence District, "Subsidence '81" (1981).
- Helm, D.C. (1975). "One-dimensional Simulation of Aquifer-system Compaction near Pixley, California. 1, Constant Parameters." *Water Resources Research*, 11(3), 465-478.
- Jacob, C.E. (1940). "On the Flow of Water in an Elastic Artesian Aquifer." *American Geophysical Union Transmittal, 21st Annual Meeting, Part 2*, 574-586.
- Jorgensen, D.G. (1975). "Analog Model Studies of Ground Water Hydrology in the Houston District, Texas." *U.S. Geological Survey, Report 190*.
- Kreitler, C.W. (1977). "Fault Control of Subsidence, Houston, Texas." *Groundwater*, 15(3), 203-214.
- Lasdon, L.S., and Waren, A.D. (1989). *GRG2 User's Guide*, Department of Management Science and Information Systems, University of Texas at Austin, Austin, TX.
- Leake, S.A., and Prudic, D.E. (1991). "Documentation of a Computer Program to Simulate Aquifer-system Compaction Using the Modular Finite-difference Ground-water Flow Model." *U.S. Geological Survey Techniques of Water Resources Investigations*, Book 6, Chapter A2.
- Marsily, G.de (1986). *Quantitative Hydrogeology - Groundwater Hydrology for Engineers*, Academic Press, San Diego, CA.
- Spyglass Transform Quick Test and Reference, Version 1.0 (1990), Spyglass, Champaign, IL.

McDonald, M.G., and Harbaugh, A.W. (1988). "A Modular Three-dimensional Finite-difference Ground-water Flow Model." *U.S. Geological Survey Techniques of Water Resources Investigations*, Book 6, Chapter A1.

Mendenhall, W., Scheaffer, R. L., and Wackerly, D. D. (1986). *Mathematical Statistics with Applications*, Duxbury Press, Boston.

Meyer, W.R. (1979). "A Digital Model for Simulation of Ground-Water Hydrology in the Houston Area, Texas." *Texas Department of Water Resources*, Report LP-103.

Peralta, R.C., and Datta, B. (1990). "Reconnaissance-level Alternative Optimal Ground-water Use Strategies." *Journal of Water Resources Planning and Management*, ASCE, 116(5), 676-692.

Poland, J.F. (1985). *Guidebook to Studies of Land Subsidence due to Ground-Water Withdrawal*, United Nations Educational, Scientific and Cultural Organization, Chelsea, Michigan.

Riley, F.S. (1969). "Analysis of Borehole Extensometer Data from Central California", in Tison, L.J., ed., *Land Subsidence*, Vol. 2. *International Association of Scientific Hydrology, Publication 89*, 423-431.

Ryder, P.D. (1988). "Hydrogeology and Predevelopment Flow in the Texas Gulf Coast Aquifer System." *U.S. Geological Survey Water Resources Investigation Report 624-B*.

*Spyglass Transform Quick Tour and Reference, Version 1.0* (1990), Spyglass, Champaign, IL.

*SURFER Reference Manual, Version 4 (1990)*, Golden Software, Golden, CO.

Terzaghi, Karl (1925). *Erdbaumechanik auf Bodenphysikalischer Grundlage* Wein  
Leipzig, Deuticke, 399.

Wanakule, N., Mays, L.W., and Lasdon, L.S. (1986). "Optimal Management of Large-  
scale Aquifers: Methodology and Applications." *Water Resources Research*, 22(4), 447-  
465.